

Table 1. Companions to Hipparcos Halo Stars

Hip. #	NLTT (1)	NLTT (2)	θ ''	p.a. deg	M_V (1)	V (1)	$V-J$ (1)	M_V (2)	V (2)	$V-J$ (2)	π	$\sigma(\pi)$
3187 ^a	2163	2167	27.7	19.5	4.8	9.88	1.19	14.0	19.04	4.95	9.70	1.30
15126 ^a	10356	10349	78.4	132.7	5.7	10.23	1.33	10.3	14.83	3.21	12.64	1.66
40068	18931	18924	110.4	208.5	3.0	10.01	1.31	7.7	14.75	2.22	3.91	1.22
43490	20570	20571	37.3	182.3	5.3	9.55	1.16	7.2	11.46	1.72	14.10	0.91
89523 ^a	46270	46279	110.6	32.5	5.5	10.13	1.36	10.7	15.31	3.78	12.04	1.07
911	525	526	8.7	168.9	-9.0	11.80	0.97	-9.0	14.35	2.16	6.13	5.67
15396	10536	10548	185.7	85.5	-9.0	11.22	0.98	-9.0	15.78	2.29	3.78	2.27
16683	11300	11288	223.5	263.6	-9.0	11.42	1.18	-9.0	14.64	2.15	5.89	2.77
52854	25404	25403	25.9	296.0	-9.0	11.43	1.19	-9.0	13.01	1.69	10.25	7.79
60849	30838	30837	15.7	23.9	-9.0	12.55	1.13	-9.0	19.09	3.03	-3.11	5.66
65418	34019	33984	490.6	84.4	-9.0	12.18	1.07	-9.0	16.10	2.26	2.52	3.57

Note. — a = indicates binaries that straddle disk-halo boundary

Disk and halo wide binaries from the Revised Luyten Catalog: probes of star formation and MACHO dark matter

Julio Chanamé and Andrew Gould

Department of Astronomy, The Ohio State University, Columbus, OH 43210, USA

jchaname, gould@astronomy.ohio-state.edu

ABSTRACT

We present a catalog of 1147 candidate common proper motion binaries selected from the revised New Luyten Two-Tenths Catalog. Among these, we then identify 982 genuine physical pairs using the measured proper-motion difference and the relative positions of each binary's components on a reduced proper-motion (RPM) diagram. The RPM positions also serve to classify them as either disk main-sequence (797), halo subdwarf (109), or pairs containing at least one white dwarf (76). The disk and halo samples are complete to separations of $\theta = 500''$ and $\theta = 900''$, which correspond to ~ 0.1 pc and ~ 1 pc, respectively. At wide separations, both distributions are well described by single power laws, $dN/d\theta \propto \theta^{-\alpha}$: $\alpha = 1.72 \pm 0.07$ for the disk and $\alpha = 1.53 \pm 0.10$ for the halo. The fact that these distributions have similar slopes (and similar normalizations as well) argues for similarity of the star-formation conditions of these two populations. The fact that the halo binaries obey a single power law out to ~ 1 pc permits strong constraints on halo dark-matter candidates. At somewhat closer separations ($10'' \lesssim \theta \lesssim 25''$), the disk distribution shows a pronounced flattening, which is detected at very high statistical significance and is not due to any obvious systematic effect. We also present a list of 11 previously unknown halo stars with parallaxes that are recognized here as companions of Hipparcos stars.

Subject headings: Galaxy: kinematics and dynamics – stellar dynamics

1. Introduction

Binaries form under the influence of their original star-cluster environment, including both stars and gas, but after the dissolution of their parent cluster, they remain mostly undisturbed during their subsequent many-Gyr voyages through the Galaxy.

There are a few exceptions to this rule. If one or both members evolve off the main sequence (MS), then the accompanying mass loss (or mass transfer) can influence the orbit. Very close binaries can circularize due to tidal interaction. Very wide binaries are so weakly bound that they can be significantly disturbed, even disrupted, by the extremely weak perturbations from inhomogeneities in the Galactic potential due to stars, molecular clouds, dark objects, or large-scale tides. Wide binaries of unevolved stars are clearly subject to only the last of these three effects.

A carefully chosen sample of wide binaries can therefore shed light both on their process of formation and the graininess of the Galactic potential through which they travel. To be useful, the sample need not be complete, it need only be free of strong selection effects as a function of projected separation. It would be of particular interest to obtain substantial samples of disk and halo binaries using the *same* selection procedure. These two populations may have formed under very different conditions and they have subsequently probed very different parts of the Galactic potential. Hence, comparison of the binary distribution functions of disk and halo samples chosen by the same procedure could help throw important light on both populations.

To date, the wide-binary distribution function has been measured by two closely related methods: two-point correlation and common proper motion (CPM). The first approach relies entirely on photometric data. One first measures the overall density of stars within a catalog of known completeness properties and then measures the excess of near neighbors as a function of angular separation relative to the background expected from random unassociated “optical pairs”. Since the density of optical pairs per unit separation θ grows $\propto \theta$, this method would appear to fail as soon as the number of real pairs in a θ bin falls below the square-root of the number of the optical pairs. In fact, the method can be pushed slightly farther by using two-band photometric data: one can require that the two components have the same photometric distance based on the assumption that both are on the MS. Of course, this eliminates real pairs with one component that is white dwarf (WD) or a giant star, but it reduces the background by a factor of a few. The same photometric distances can then be used to determine the binary’s physical separation, a , from its angular separation, θ . Bahcall & Soneira (1981) pioneered this method, obtaining a list of 19 candidate pairs from a sample of 3000 stars assembled by Weistroop (1972). Gould et al. (1995) applied this technique to a sample drawn from *Hubble Space Telescope* data to obtain 13 candidate pairs, and based on this made the first estimate of the relative rate of disk and halo wide binaries from a single homogeneous sample. Garnavich (1988, 1991) attempted to apply this technique to a much larger sample, but obtained puzzling results that are inconsistent with all other surveys. See the Appendix of Gould et al. (1995). Once candidates are found using the two-point correlation technique, they can be confirmed by radial velocity (RV) measurements, as was

done by Latham et al. (1984) for some of the stars in the Bahcall & Soneira (1981) sample.

The second (CPM) method adds proper-motion information to the positional astrometry and photometry of the first. Because of their wide separations and corresponding low orbital velocities, wide binaries should have very similar proper motions and, if these are available, they can be used to distinguish genuine binaries from much more numerous pairs of unassociated stars in the field. Of course, the technique does break down at sufficiently large separations, primarily because the number of field stars eventually becomes so large that some unassociated stars actually have similar proper motions, but ultimately because at sufficiently large separations, the observed proper motions represent substantially different projections of the common physical velocity. Wasserman & Weinberg (1989) applied this technique to the Woolly catalog and, after vetting their sample using RV measurements, Close, Richer & Crabtree (1990) obtained a sample of 32 wide binaries.

Multiplicity studies as a function of stellar type in the Galactic-field population include the works of Duquennoy & Mayor (1991) for G dwarfs and Fischer & Marcy (1992) for M dwarfs. These two important works combine observational techniques that operate on different regimes of angular separation to assemble volume-limited samples of binaries spanning more than 10 decades of orbital period. While both studies find similar period distributions for these spectral types (showing a Gaussian-type shape as a function of $\log P$ with a broad peak centered around $P \sim 40$ yr, or equivalently $a \sim 25$ AU), the M-dwarf binary frequency ($\sim 42\%$) is lower than that of G dwarfs ($\sim 57\%$), although this could be due to the somewhat different ranges of companion masses for the two samples. Pre-MS stars, however, seem to differ significantly. Several surveys of T Tauri stars ($\lesssim 5$ Myr) in nearby star-forming regions like Taurus-Auriga, Ophiucus-Scorpius, Chameleon, Lupus, and Corona Australis, find a binary fraction about twice as large as that of field stars (Ghez, Neugebauer, & Matthews 1993; Leinert et al. 1993; Simon et al. 1995; Ghez, McCarthy, Patience, & Beck 1997; White & Ghez 2001). There is, nevertheless, one interesting exception, the Orion Nebula cluster (ONC), for which Petr et al. (1998) find a binary fraction in agreement with that of MS field stars (see also Prosser et al. 1994; Scally, Clarke, & McCaughrean 1999; and Duchêne 1999). Since the ONC is different than the other surveyed star-forming regions in that it has a much higher stellar density, this result suggests an environmental dependence of the binary fraction among pre-MS stars.

Recent works have focused on the binary properties of MS populations as a function of age and environment, and their comparison to what is observed in the field. While the comparison between T Tauri and Galactic field populations reveals a discrepancy between the measured binary fractions of pre-MS and old MS stars, multiplicity studies in stellar clusters with young MS populations such as α Persei (~ 90 Myr), the Pleiades (~ 120 Myr),

and the Hyades and Praesepe (~ 660 Myr) find a binary fraction consistent with that of the corresponding range of separations among the older G and M dwarfs in the field. Thus, the binary frequency appears not to decline with age on timescales from ~ 90 Myr to ~ 5 Gyr (Bouvier, Rigaut, & Nadeau 1997; Patience et al. 1998; Patience, Ghez, Reid, & Matthews 2002).

None of the above works, however, has attempted the construction and subsequent comparison of complete samples of binaries unambiguously belonging to the disk and halo of the Galaxy. The difficulty in assembling statistically significant samples of binaries with well-understood selection effects, together with the requirement of obtaining the information necessary to classify the stars as belonging to either population, must have certainly worked against this goal. Nevertheless, a few important efforts to obtain samples of either disk or halo binaries should be mentioned. First, in the most recent report of a large spectroscopic survey of high proper-motion stars, Latham et al. (2002) find no difference in the binary frequency and period distribution of two samples of (93) disk and (78) halo binaries. These are, however, close binaries with periods of less than 20 yr (their spectroscopic monitoring started in 1987) or, equivalently, semi-major axes $a \lesssim 7$ AU. Ryan (1992) obtained optical photometry of a number of CPM pairs selected from the New Luyten Two-Tenths (NLTT) Catalog, which he determined to belong to the Galactic halo. Since a fraction of his binaries are common to the present work, we leave the discussion of this paper to §5.3. Also, Allen, Poveda, & Herrera (2000) searched in NLTT for CPM companions of a sample of high-velocity and metal-poor stars taken from another source, finding 122 binaries. Here we only note that this corresponds to just $\sim 10\%$ of all the wide binaries available in NLTT, and discuss the Allen et al. (2000) work in detail in §5.3.

From this summary (see also Appendix of Gould et al. 1995), it appears that obtaining a large sample of wide binaries is a formidable task. Generally surveys are sensitive to only about 2 decades of separation, being bounded by merging images at the close end and by confusion with unassociated field stars at the wide end. The total fraction of stars with wide companions is only a few percent per decade of separation, and within a given survey many of these may be lost due to the magnitude limits of the survey.

The NLTT Catalog (Luyten 1979, 1980; Luyten & Hughes 1980) would seem to be an obvious source of wide binaries. NLTT is a proper-motion limited catalog ($\mu > 180$ mas yr $^{-1}$), which is largely complete over 19 magnitudes. It contains photographic photometry in two bands for the great majority of its almost 59,000 entries. Most importantly in the present context, it is appended by a set of notes which, in particular, identify pairs believed by Luyten to be CPM binaries. It would probably have been possible to carry out a complete search of wide binaries in NLTT, and it is not completely clear to us why no one has attempted to

do this, since the sample obtained would be several orders of magnitude larger than those previously listed. However, we do note several obstacles that would have had to have been overcome. First, the NLTT photographic colors are quite crude and so do not permit the construction of a reliable reduced proper motion (RPM) diagram (Salim & Gould 2002). Hence, the NLTT photometry is only marginally useful in discriminating genuine binaries from random field pairs. Second, for most cases for which Luyten believed that a pair was a CPM binary, he did not record his independent proper-motion measurements. Instead he assigned both stars the same proper motion. As we show below, a significant fraction of the widest binaries ($\theta \gtrsim 100''$) so recorded are not genuine pairs, but rather are unassociated stars with substantially different proper motions. However, because Luyten did not record his measurements, there is no way to identify these except by remeasuring their proper motions. Third, Luyten failed to identify a number of genuine binaries at wide separations because his measurement errors of $\sigma \sim 20 \text{ mas yr}^{-1}$ (Salim & Gould 2003) did not permit him to reliably distinguish these from the numerous unrelated optical pairs at these separations. Thus, considerable additional work would have been required to extend an NLTT-based sample into the range $\theta \gtrsim 100''$.

With the publication of the revised NLTT (rNLTT) by Gould & Salim (2003) and Salim & Gould (2003), all three of these problems can be overcome. For the 44% of the sky covered by the intersection of the first Palomar Observatory Sky Survey (POSS I) and the Second Incremental Release of the Two-Micron All-Sky Survey (2MASS Skrutskie et al. 1997), rNLTT has optical-infrared photometry for the great majority of NLTT stars, and this is sufficient to permit good stellar classification using an RPM diagram (Salim & Gould 2002). The roughly 3-fold increase in temporal baseline of rNLTT relative to NLTT permits a substantial improvement in proper-motion accuracy to $\sigma \sim 5.5 \text{ mas yr}^{-1}$. Moreover, the accuracy of *relative* proper motions of nearby stars (which is what is relevant to the problem of CPM binaries) is even better: $\sigma \sim 3 \text{ mas yr}^{-1}$. This means that the vector proper motion measurements of real pairs typically differ by only 6 mas yr^{-1} (Salim & Gould 2003). Finally, rNLTT contains entries comparing Luyten’s original (circa 1950) estimate of the vector separation of the binary components with rNLTT’s own (circa 2000) measurement, and these can be compared to help identify spurious CPM binaries.

Nevertheless, it is by no means straightforward to assemble a uniformly selected catalog of wide binaries from the rNLTT. First, for binaries with separations $\theta \lesssim 10''$, rNLTT often fails to identify both companions because its underlying sources, mostly USNO-A (Monet 1996, 1998) and 2MASS, can be blended at these close separations. Even at wider separations, NLTT stars can be missing from one or both of USNO-A and 2MASS for a variety of reasons, including crowding, saturation, as well as other often unidentifiable effects. If it is missing from both, then the NLTT star is not in rNLTT. If it is missing

from one, then rNLTT does not have an independent proper motion. Finally, the Second Incremental 2MASS release has almost fractal sky coverage. Hence, one component of a binary might be in rNLTT and the other not simply because they lie on opposite sides of this very complicated boundary. Since the probability of this happening increases with separation, it must be carefully investigated.

Here we assemble a catalog of wide rNLTT binaries. In proper motion surveys, binaries are identified by means of the CPMs of their components, which in rNLTT are measured over a timescale of about 45 years (the time between the acquisition of the POSS-I plates and the 2MASS survey). These binaries have not appreciably changed their apparent separation on the sky in half a century, so their orbital periods are almost all longer than several hundred years, corresponding to semi-major axes above about 100 AU.

We take a variety of steps to systematically minimize all the potential problems described above. We classify binaries as either disk or halo, and extend our search to separations $\theta < 500''$ for disk binaries and $\theta < 900''$ for halo binaries. These correspond to physical separations of about 0.1 pc and 1 pc respectively. We find that both distributions of angular separations are characterized by power laws $f(\theta) \equiv dN/d\theta \propto \theta^{-\alpha}$, with $\alpha = 1.72 \pm 0.07$ and $\alpha = 1.53 \pm 0.10$ respectively. That is, the slopes are consistent with each other at the 1.6σ level. We also find that the normalizations are reasonably consistent. The two populations of wide binaries are also similar respecting their distributions of luminosity and mass ratios. Our main conclusions are therefore that disk and halo binaries probably formed under similar conditions, and that the metallicity of the environment does not affect the outcome of the process of star-formation on large scales.

Furthermore, we find no evidence of any falloff in the number of binaries at the largest separations with respect to these power laws. Since the widest binaries are easy to disrupt in encounters with other objects, our results allow for the possibility of establishing limits on the density of massive dark objects in the Galactic halo. Such limits are derived in a companion paper (Yoo, Chanamé, & Gould 2003).

We note here that, although the binaries studied in this work are all of wide physical separations ($a \gtrsim 100$ AU), throughout this paper and for reasons of convenience that will become clear in §2 and §3, we subdivide our dataset into “close” and “wide” subsamples, according to whether their angular separations on the sky are smaller or larger than $10''$.

The structure of the paper is as follows. In §2 we describe the limits of our search for CPM systems and the selection of the candidate pairs. These are then classified in §3 as either genuine disk or halo binaries. The characteristics of the final clean samples are studied in §4, where we also derive the distributions of angular and physical separation, as well as

the distributions of luminosity and mass ratio. In §5 we discuss our findings, and we present our conclusions in §6. The catalog description is given in Appendix A, and in Appendix B we present a list of 12 previously unknown halo stars with parallaxes that are recognized in this work as probable companions of Hipparcos stars. The catalog in ascii format can be retrieved from http://www.astronomy.ohio-state.edu/~gould/rNLTT_binaries/binaries.dat.gz.

2. Sample Selection

2.1. Overview

Our overall strategic aim is to assemble a catalog of all genuine wide binaries that satisfy three conditions. First, both components are catalogued in NLTT. Second, at least one component is in the intersection of POSS I and the 2MASS Second Incremental Release, i.e., the area over which rNLTT attempted to be complete. Third, the separation is restricted to the range $\theta < 500''$ for disk binaries and $\theta < 900''$ for halo binaries. We also exclude all triples. Of course, one would like to incorporate high proper-motion binaries with one or both components missing from NLTT, but there are at present no publicly available data from which these could be identified with a reasonable amount of work.

To achieve this aim, we first investigate all pairs identified as binaries in the NLTT notes (hereafter “Luyten binaries”) to determine if they are genuine and then check all other pairs up to the maximum separation to determine whether any of these are also genuine binaries. At first sight, it may appear that the division into Luyten and non-Luyten binaries is superfluous. However, as we will soon show, there is a wealth of information on the Luyten binaries that is not available for the non-Luyten binaries, so we are really quite fortunate that Luyten was very systematic in identifying binaries.

We then divide the 1073 Luyten binaries into two broad classes, “close” and “wide” according to whether Luyten measured their separation as $\theta \leq 10''$ or $\theta > 10''$. These contain respectively 37% and 63% of the sample. This division is motivated by two considerations. First, the close binaries can be regarded as real because the chance of two unassociated stars lying so close in both position and velocity space is small: only of order one such spurious binary is expected in the entire rNLTT catalog. (Indeed, we searched for pairs within $10''$ that Luyten did not call “binaries” and found only one. We confirmed that this one was indeed an unassociated pair.) Second, the rate of non-identifications in USNO-A and 2MASS is much higher among the close than the wide binaries, so this is a natural division from the standpoint of classifying binaries in the sample. That is, for the close binaries, we simply assume that they are all genuine, and focus our efforts on classification (§ 3.1), while for the

wide binaries, we assemble all the available information to first determine if they are good CPM candidates (§ 2.2) and then to classify them (§ 3.2).

2.2. Wide Luyten Binaries, $\theta > 10''$

We begin the vetting of Luyten wide binaries by plotting the absolute value of the vector proper-motion difference of the components against separation. We adopt the notation $\Delta\mu = |\Delta\mu|$. See Figure 1. It goes without saying that binaries can only be plotted on this diagram if both components have proper motions independently measured by rNLTT. However, this simple criterion fails for 136 of the 679 wide Luyten binaries for one of the following reasons: neither component in rNLTT (4), one component not in rNLTT (38), one component lacking a proper motion because it is identified only in 2MASS (84), one component lacking a proper motion because it is identified only in USNO-A (10).

Fortunately, it is still possible to obtain independent proper-motion measurements for the largest subcategory, the 84 stars with 2MASS-only identifications in rNLTT. These stars were originally identified in rNLTT by searching in 2MASS for the companion to an already identified rNLTT star at the position offset given by the NLTT notes. Salim & Gould (2003) showed that these position offsets are generally accurate to ~ 600 mas, although there are some outliers (see their fig. 8). Hence, by comparing the vector difference in epoch 2000 positions from rNLTT with the vector offset given in the NLTT notes, we obtain a proper-motion estimate with an error of 600 mas/45 yr ~ 13 mas yr $^{-1}$. Moreover, by performing the same type of search among the 38 binaries with only one component in rNLTT, we find an additional 2 2MASS-only companions that were evidently missed by Salim & Gould (2002).

We select stars as good candidates for further investigation according to whether they fall above or below the dashed line in Figure 1. At wide separations, this curve is set at $\Delta\mu = 20$ mas yr $^{-1}$, corresponding to the 3σ error in proper-motion differences (except for the 2MASS-only stars). At closer separations, we are more tolerant of large proper-motion differences, partly because the chance of contamination by unassociated pairs is lower and partly because some pairs at close separations can have significant orbital motions. In fact, by individually exploring all the pairs in Figure 1 that show proper-motion differences larger than the imposed cut, but have separations smaller than $50''$, we identify 5 cases for which the large $\Delta\mu$ is due to orbital motions, and these are indicated as red stars. We further discuss this selection in § 2.3, below.

We search for each of the remaining $38 - 2 = 36$ unidentified companions to rNLTT stars in USNO-B (Monet et al. 2002). Gould (2003a) showed that this catalog is about 90%

complete for high proper-motion stars and that its internally reported errors are generally accurate. The catalog cannot be used to search in the field for high proper-motion stars because about 99% of its high proper-motion entries are spurious. However, it can be used to look for individual high proper-motion stars at known locations. Of these 36 companions, we find 16 in USNO-B, and exclude 2 of these on the grounds of large proper-motion difference between the components. Finally, among those not found in USNO-B, we exclude the 6 widest pairs ($\theta > 200''$) since no proper-motion difference between their components can be established.

The remaining 14 binaries whose secondaries could not be identified either in 2MASS or USNO-B need to be handled carefully, since the primary may have been falsely identified by rNLTT. We deal with these in § 3.2 where we include classification criteria to assess their reality. Here we just remark that 4 from this group make it into our final clean sample.

We search in USNO-B for the 10 wide pairs with a component lacking a proper motion because it is only identified in USNO-A but not in 2MASS, and find all of them. Eight of these pairs are confirmed to be CPM systems, while the other 2 have large proper-motion differences and are excluded from the sample.

Finally, 8 binaries lack 2MASS photometry for both components, even though there are entries for them in this survey. The 16 stars in these pairs are very bright Tycho objects that saturated the 2MASS detectors. With 2 exceptions, we confirm the reality of these pairs as CPM systems by comparing images at two different epochs (ESO Online Digitized Sky Survey, <http://archive.eso.org/dss/dss>). In § 3.2 we will assign these six binaries to the disk population, because of the brightness of both their components.

Note that the exclusion from the analysis of pairs outside the allowed region of the $\log \theta - \Delta\mu$ plane does not mean that all these systems should be regarded as false binaries. Rather, it reflects our philosophy of being as complete and free of selection effects as possible, but at the same time rigorous in not being contaminated by unrelated optical pairs. CPM systems excluded by this cutoff, especially those at large apparent separations, are good candidates for radial velocity follow-up in order to determine their reality.

2.3. Non-Luyten Binaries

Figure 1 also shows all pairs of rNLTT stars that satisfy the following three conditions. First, they are not listed as binaries in the NLTT notes. Second, they have rNLTT proper-motion differences $\Delta\mu < 40 \text{ mas yr}^{-1}$. Third, they have separations $\theta < 500''$. Among halo stars, we also show those with separations up to $900''$ and $\Delta\mu < 20 \text{ mas yr}^{-1}$. The density

of unassociated pairs scales $d^2N/d\theta d\Delta\mu \propto \theta \Delta\mu$. Hence, one expects the unassociated pairs to be concentrated near $\Delta\mu \sim 40 \text{ mas yr}^{-1}$ and $\theta \sim 500''$, while the real binaries should hover about the x-axis. When the Luyten and non-Luyten pairs are combined, this expected behavior is evident. It is clear that Luyten did indeed miss some binaries, which we extract by imposing the same selection indicated by the dashed curve. It is also clear from the figure that we cannot push our sample too far beyond $\theta = 500''$ without risking serious contamination. We will discuss this point further in § 3.2.

Note that in order for non-Luyten binaries to make it into our sample, both components must have independent rNLTT proper-motion measurements. For comparison, of the 679 wide Luyten binaries, 134 had at least one companion initially lacking such a proper-motion measurement. However, for 89% of these, we were able to *use the information from the NLTT notes* that a companion existed as well as its approximate offset, to actually locate the companion. That is, we have high-precision relative proper-motion measurements for 98% of the 679 wide Luyten binaries. However, if NLTT stars have other NLTT stars as genuine binary companions, but these are not recovered by rNLTT, we have no way to identify them by searching in rNLTT alone. Fortunately, we can use USNO-B to search for this last subset of non-Luyten binaries. The results of this search are discussed in §3.2.

3. Classification: Disk Versus Halo Binaries

The large size of the binary sample selected in § 2 is by itself a significant improvement over previous efforts. However, our main motivation is to exploit the unprecedented capability of rNLTT to cleanly separate local disk and halo populations. These two advantages combine to give us, for the first time, complete and unbiased samples of wide binaries belonging to stellar populations whose formation and evolution remain as open questions in Galactic astronomy. In this section we describe our classification methodology. We also show how this procedure permits the identification of the few unrelated pairs and bad matches that slipped through the selection criteria of § 2.

We separate the disk and halo populations using the RPM discriminator η introduced by Salim & Gould (2003),

$$\eta = V_{\text{RPM}} - 3.1(V - J) - 1.47 |\sin b| - 2.73, \quad (1)$$

where

$$V_{\text{RPM}} = V + 5 \log \mu, \quad (2)$$

is the RPM, μ is the proper motion of the star in arcsec per year, b is its Galactic latitude, and $V - J$ and V are its color and magnitude. Basically, we classify stars as disk or halo according to whether η is negative or positive.

To understand how the RPM discriminator η works, we examine each term separately. The RPM is $V_{\text{RPM}} = M_V + 5 \log(v_{\perp}/47.4 \text{ km s}^{-1})$, where v_{\perp} is the transverse speed. Hence, the RPM is a proxy for the star's intrinsic luminosity: if all stars had the same speed, the RPM would equal the absolute magnitude M_V up to an additive constant. Since halo stars typically move about 5 times faster than disk stars and since they are typically a magnitude or two fainter at fixed color, their RPMs are typically about 5 magnitudes greater than those of disk stars. Hence, despite the considerable dispersions in V_{RPM} for each population, the halo and disk tracks are well separated on a RPM diagram (see Salim & Gould 2002 and Figure 2 in the present paper).

The second term, $3.1(V - J)$ is approximately the slope of the “blank track” between the two tracks populated by the disk main sequence (MS) and the halo subdwarfs (SDs). That is, the equation of this blank track is $V_{\text{RPM}} = 3.1(V - J) + \text{const}$. However, as demonstrated by figure 2 of Salim & Gould (2003), this constant is actually a function of Galactic latitude b . At higher latitude, the transverse motions of both halo and disk stars are larger than at low b . This is partly because of their asymmetric drift in the tangential direction and partly because of their higher dispersion in the radial direction. The third term takes account of this effect. The last term is included for convenience, that is, so that $\eta = 0$ at the boundary.

In fact, η discriminates not only between MS stars and SDs but also WDs: stars are classified as disk if $\eta < 0$, as halo if $0 < \eta < 5.15$, and as WDs if $\eta > 5.15$.

When classifying the binaries, one expects not only to find that both components belong to the same population, but also that their positions on the RPM diagram lie on the same “isochrone”. That is, since the two members of a binary must have similar metallicities and essentially the same proper motion but usually different luminosities, one expects that the line connecting their positions on the RPM diagram should be approximately parallel to the corresponding MS or SD track for disk and halo binaries, respectively. See figure 12 of Salim & Gould (2003). Hence, by placing both components of the binary on an RPM diagram, we not only classify it as disk or halo, but also subject it to an extra test of the physical association of the two components. Naturally, the only cases permitted not to follow this “parallel rule” will be those involving a WD companion. Binaries composed of one MS and one SD member will be rejected as unrelated pairs. So will binaries composed of two MS or

two SD stars if the line connecting them is inconsistent (within measurement errors) of being parallel with the respective sequence. In a very few cases, we find that the connecting line straddles the disk/halo boundary, being consistent within measurement errors of being either a disk or a halo binary. These binaries are excluded from the sample because this ambiguity does not allow us to reliably classify them with the present data. Figure 2 illustrates various classification examples, including good disk and subdwarf binaries, cases of uncertain type, as well as pairs rejected because of inconsistent membership.

Our philosophy is to effectively use all the information available for each star in order to assign it to the disk or halo population, or identify it as a WD. According to the amount of information available, we then construct several subgroups and study them separately. Just as during sample selection, we consider close and wide binaries as independent subsets. Inside any of these subgroups, we typically must close-inspect several pairs to figure out the source of either discrepant classifications or pairs containing MS and subdwarf members. Whenever the source of the anomaly cannot be determined, the pair is rejected.

The following subsections contain a detailed account of the classification process for each subgroup of binaries and the final tally of disk and halo memberships. Some readers may wish to skip to § 4, where we present our results.

3.1. Close Binaries

Very close binaries are affected by blending, thereby corrupting the RPMs, colors, and RPM discriminators η of their components as they are derived from rNLTT. For example, suppose USNO-A could not resolve a binary whose components have similar luminosities. These then would appear in rNLTT as having equal V magnitudes, but too bright by 0.75 mag. Depending on whether or not the stars were also unresolved in 2MASS, their colors could be incorrect as well, leading to values of η that could send one or both components to the incorrect side of the RPM diagram and hence be either rejected as a false match or erroneously classified. With this in mind, we perform a first subdivision of the close binaries into four subgroups according to whether their components are resolved or blended by the 2MASS and USNO photometry. Additionally, there are four other subgroups according to whether the binary is resolved or not by 2MASS and whether one or both of the binary’s components do not have a match in the USNO scanned plates. Next we go one by one through these subgroups and detail the classification scheme.

2MASS and USNO resolved binaries [22]. These binaries have all the possible information available, so no assumption has to be made in their classification. We compute η for all the

stars using both the USNO-A photometry as well as the Luyten photometry and obtain the same classification in every single case. This is relevant because it gives confidence for using Luyten photometry in the cases for which USNO-A data are blended or not available. One binary is rejected because its components were classified as disk and subdwarf.

2MASS resolved and USNO blended binaries [43]. These binaries, although blended in USNO-A, were resolved by Luyten. Prompted by the good results given by the Luyten photometry when the USNO-A data are resolved (previous subgroup), we compute η using the resolved data from Luyten. Additionally, we merge the 2MASS resolved detections and, combine them with the blended USNO-A measurement, and so compute η for the “merged binary”. There are only two cases for which the Luyten photometry and the merged binary give different answers, and we choose to follow the former one. There are no disk-subdwarf cases in this subgroup.

2MASS blended and USNO resolved binaries [1]. As 2MASS has better angular resolution than USNO-A, these should be rare. Indeed, the one example is a very special case. The two components are very faint, with Luyten magnitudes of $V \sim 19$ and 18, and with the brighter component being very blue both in the Luyten and USNO-A colors, hence indicating a WD.

2MASS and USNO blended binaries [128]. For these binaries we compute η for the merged binary, and compare it with the value obtained from the 2MASS blended measurement and the optical magnitude obtained by merging the resolved Luyten measurements. In 11 of the cases ($\sim 9\%$) we find disagreement between these classifications. We examine each of these individually in order to determine the origin for the disagreement and so assign the most appropriate classification. There are also 9 cases of disk-subdwarf pairs, which are due to relatively large proper-motion differences and the proximity of these binaries to the $\eta = 0$ boundary between the two populations.

2MASS resolved and one component missing in USNO [90]. For this subgroup we compute η for the component with USNO-A data, and for both components using the resolved Luyten photometry. There are 11 cases for which both classifications for the component having USNO-A data disagree and 13 cases of disk-subdwarf pairs from the Luyten classification. Close inspection of the 11 disagreements favors the results from the Luyten photometry in all cases, so these are adopted. The 13 disk-halo pairs are rejected.

2MASS resolved and both components missing in USNO [53]. In these cases the only optical photometry available is Luyten’s, so we use it to compute η for all components. We find only 4 cases are classified as disk-subdwarf, and we reject them.

2MASS blended and one or both components missing in USNO [17]. Here the only alternative is to combine the optical light given by the Luyten photometry and classify the merged binary

as if it were a single star. Except for one binary with a probable WD component, all the rest are classified as disk binaries.

One component not in rNLTT [34]. As with the cases discussed in §2.2, we search for the companions of these rNLTT stars in USNO-B, finding only 2 matches. The remaining 32 binaries are classified following the component present in rNLTT, and also verifying that the NLTT colors are consistent with the components lying on the same isochrone. In this way 15 are classified as disk binaries, 4 as halo binaries, and 11 are disk pairs with a WD component. The remaining 2 binaries in this category have uncertain classifications and are not included in the final samples.

Neither component in rNLTT [7]. These were found by searching in the intersection between the Luyten notes and NLTT stars that nominally lie in 2MASS areas but were not recovered by rNLTT. We accept only those pairs that have 2MASS measurements, whose 2MASS separations and position angles are consistent with the Luyten notes, and whose 2MASS entries do not have USNO-A counterparts, which would indicate a slow-moving star. Four of these 7 are considered real binaries based on their RPMs, of which 2 contain a WD component.

While our philosophy is to accept all 395 close binaries ($\theta < 10''$) as genuine, 32 systems could not be cleanly classified and are removed from the sample. Of the remaining 363 systems, 62 are classified as halo binaries, 282 as disk binaries, and 19 contain a WD companion.

3.2. Wide Binaries

Wide binaries are not as problematic as close binaries since they are not usually affected by blending. However, we still have to deal with cases for which one or both components lack USNO-A and/or 2MASS data, or for which one or both components are missing from rNLTT. Moreover, in contrast to the close binaries, we do not automatically accept the wide binaries as genuine, but rather demand that both components sit on the same isochrone as described in § 3.

Whenever USNO-A photometry is not available, we derive the V magnitude from Luyten photometry, which was shown to be a safe procedure in the previous section (the 23 binaries resolved in both 2MASS and USNO yielded the same classifications regardless of the use of USNO-A or Luyten photometry). Of our wide binaries 654 (88%) have 2MASS data for both components, and hence their classification is straightforward. For the 43 wide binaries having one component missing in 2MASS, we follow the disk/halo classification obtained

from the component with a near-IR measurement and check that the Luyten photometry is consistent with the two stars lying approximately on the same isochrone. Finally, 6 binaries lack 2MASS measurements for both components but were confirmed as CPM systems in § 2.2. The 12 stars in these pairs are very bright Tycho-2 objects that saturated the 2MASS detectors, and are all assigned to the disk population.

As explained in previous sections, binaries with one component missing from rNLTT are individually searched for in USNO-B. Of the 38 wide pairs in this category, the missing component of 16 are found in USNO-B and easily classified. Two of the binaries with rNLTT-missing companions not found in USNO-B are then found in 2MASS and classified, and another 6 that are part of very wide systems ($\theta > 200''$) are excluded because no information on their proper-motion difference is available to judge their reality. For each of the remaining 14 binaries, we closely inspect the Luyten photometry on both components, finding 5 pairs with a WD component and confirming the other 9 as being approximately on the same isochrone. We furthermore examine them in online (ESO database) images at separate epochs, and visually confirm 4 pairs to be real CPM systems. These 4 are classified following the type of the component present in rNLTT. The remaining 5 pairs whose reality as CPM systems is difficult to confirm from the images are excluded from the sample.

Next, given our goal to assemble a complete catalog of all the CPM binaries present in NLTT, we also search for the subset of binaries not recognized as such by Luyten (i.e., non-Luyten binaries) and which have not been already found because one or both of its components were not recovered by rNLTT. As pointed out in §2.3, 134 of the 679 wide candidate Luyten binaries had at least one component lacking an independent proper-motion measurement. In terms of wide binaries that were accepted in the final samples, these last two numbers become 81 and 561, respectively. Based on this experience with Luyten wide binaries and scaling to the 58 wide non-Luyten binaries that we have already accepted into our final clean samples, we estimate that there are an additional $(58 \times 81)/(561 - 81) \sim 10$ non-Luyten binaries that we have missed. In order to see if we can account for these, we use USNO-B and perform a search around NLTT stars for CPM companions that are also NLTT stars, expecting to find ~ 7 given the incompleteness of USNO-B (which for binaries rises from 10% at $30''$ to 50% at $10''$; Gould 2003b). We find 3. Of these, 2 turn out to be companions of binaries already in our sample, making them triple systems, while the third one is a real pair (NLTT 1024/1041) which was missed by us because rNLTT misidentified the secondary, recovering instead an unrelated nearby object. The fact that we find 3 when we expected ~ 7 of these binaries is somewhat improbable ($\sim 8\%$). However, the remaining ~ 4 missing binaries should have a negligible impact in our sample of about a thousand binaries.

Of the $758 - 68 = 690$ wide CPM systems that passed through the selection criteria of § 2.2, 129 are excluded from the clean sample by the classification procedure described above. These 129 include 73 systems containing WD components and 56 that show either unphysical MS-subdwarf classification or inconsistent RPM positions. The final clean sample consists of 561 wide binaries with solid classification: 512 belonging to the disk population, and 49 belonging to the Galactic halo. Figure 3 shows $\sim 10\%$ of our wide binaries, selected randomly from the final clean samples.

4. Results

In this section we report on the properties of our final datasets. Our main result consists of the determination of the binary frequency as a function of the separation between the components. This distribution can be computed directly as a function of angular separation on the sky by the simple counting of the number of binaries in each interval of $\log \theta$. However, since it is also of interest to know the distribution of projected physical separations, we need to assign distances to each of our binaries. Furthermore, distances are needed in order to determine stellar masses and study the distribution of mass-ratios between the components of the binaries. We accomplish this with the use of color-magnitude relations (CMRs), derived separately for the disk and halo samples. These, although not very precise as an absolute distance indicator for any given system, can be used in a statistical way as a characterization of the distances probed and to infer several overall properties of this dataset.

In §4.1 we study the color distributions of the final samples and compare them with the underlying rNLTT catalog. In addition, color-color diagrams are used to map the range of spectral types of the stars in our datasets. We then describe in §4.2 the derivation of the CMRs that we use to determine individual distances to the binaries, showing the distributions of distances and luminosity functions of both the disk and halo samples. The distributions of angular and physical separations are presented in §4.3, and in §4.4 we show the distributions of luminosity and mass ratios between the components of the binaries.

4.1. Color distributions and spectral types

In Figure 4 we show the $V - J$ color distribution of the stars in binaries in comparison with that of the entire rNLTT catalog, for disk and halo populations separately. The rNLTT disk and halo single stars included in these plots are those whose membership to either one of these types is very secure. In terms of the discriminator η introduced in §3, secure disk

stars are those with $\eta < -1$, and secure halo stars those with $1 < \eta < 4.15$, which produces sets of 17,690 and 4,883 stars, respectively. The resulting color distributions of both sets of binaries are, with a high degree of confidence according to KS tests, different than those of the corresponding rNLTT stars. These diagrams show that both samples of binaries have larger fractions of bright (i.e., blue) stars than the catalog as a whole. This is a selection effect due to the magnitude-limited nature of rNLTT (i.e., the companions of bright stars are preferentially selected compared to those of fainter ones), and should be kept in mind when interpreting results regarding the distributions of luminosity and mass ratios.

In order to learn about their spectral characteristics, we plot in Figure 5 color-color diagrams of the stars in our binaries. Given the proximity of these samples (see §4.2 below), reddening should have a negligible effect on the main features of these diagrams. The approximate locations of dwarf stars of various spectral types are indicated, as obtained from similar diagrams by Gizis et al. (2000) and Finlator et al. (2000). Both plots indicate that the large majority of the stars in these binaries are dwarfs of spectral types between M0 and M5 (M6 dwarfs have $J - K \gtrsim 1$). Less populated tails of late G and K stars complete the datasets. Almost all the stars have $V - J \gtrsim 1$, corresponding to $M \lesssim 1 M_{\odot}$ for disk MS stars and $M \lesssim 0.8 M_{\odot}$ for subdwarfs.

4.2. Disk and halo color-magnitude relations

Of the 788 disk binaries in our final sample, 242 have at least one component catalogued in the Hipparcos database, 196 of which are wider than $10''$. In the case of the halo sample, 9 binaries have Hipparcos parallaxes available, with 7 of them being wider than $10''$. However, most of these are bright primaries, and, although their secondaries can be considered also as stars with “measured” parallaxes, they are not fully representative of either the disk or halo samples of binaries. For this reason we make use of single stars in the Hipparcos database itself, as well as halo stars present in rNLTT with parallaxes from other sources. We thereby assemble parallax samples covering the full color ranges spanned by both our disk and halo binaries.

Figure 6 shows $(M_V, V - J)$ color-magnitude diagrams (CMDs) for the parallax samples and the polynomial fits we obtain from them. The small dots in the upper panel (6a) are all Hipparcos stars within 50 pc of the Sun, which very well cover all the blue half of our disk sample. These stars show a scatter with respect to the fit of 0.41 mag, consistent with that measured by Reid (1991) for the solar neighborhood. The red half is filled with all the stars in the sample of disk binaries that are companions to Hipparcos stars, and are shown as open triangles. The scatter with respect to the fit for the red stars is 0.87 mag, much larger

than that of the first group of stars. While it is known that the scatter in the CMR depends on color and has a maximum of 0.5 mag at $V - I \sim 2.5$ ($V - J \sim 4$) (Reid 1991; Monet et al. 1992), there are still 0.7 mag that cannot be explained by the USNO-A photometric errors alone (~ 0.25 mag). We fit this MS with a 7th-order polynomial, shown as the solid line, and use this fit as our CMR for the disk sample.

Similarly, in Figure 6b we show the stars used to determine the halo CMR. The black dots are single halo stars present in rNLTT that have Hipparcos parallaxes, and the open triangles are the components of the 9 halo binaries described before. These two groups cover only the blue half of our sample of halo binaries. The red end of the subdwarf track is filled with 26 LHS stars (open circles) with parallaxes measured by Monet et al. (1992) and Gizis (1997), and that are classified as halo stars using the rNLTT data. We fit this halo CMR with a 5th-order polynomial, shown as the solid line going through the data. The dashed line is the linear CMR obtained by Gould (2003) from a kinematic analysis of 4588 subdwarfs selected from rNLTT.

Figure 7 shows the CMD for all the disk and halo binaries with separations larger than $10''$ (the wide sample) that satisfactorily passed the selection and classification procedures described in §2 and §3. The solid lines are the CMRs derived from the subsamples of rNLTT stars with parallaxes described above, and placed at convenient distances that are discussed next.

Figure 8a shows the distribution of the distances to all our primaries (in close and wide binaries) obtained with our fits to the CMRs. Note that the disk binaries are located at an average distance of 60 pc, while the halo binaries lie farther away, with an average distance of 240 pc. This is expected: since halo stars move faster than disk stars, they can be detected at larger distances in a proper-motion limited sample. Finally, using these distances we plot in Figure 8b the V -band luminosity functions (LF) for stars in disk and halo binaries (both primaries and secondaries together). The peak of the disk LF occurs at $M_V \sim 11$, which can be compared to the LF of M dwarfs obtained from HST counts, which peaks between 11 and 12 (Zheng et al. 2001). In the case of the halo, the LF of binary components appears to peak at $M_V \sim 10$, very close to what Gould (2003) found in his analysis of 4588 subdwarfs selected from the same rNLTT.

4.3. Angular separation and semimajor axis distributions

The distributions of angular separations for our final samples of (788) disk and (111) halo binaries are shown in Figure 9. Recall that our search extends to separations up to

500" for disk binaries, and 900" for halo binaries. The normalization is set relative to the entire underlying rNLTT catalog, done separately for disk and halo stars. The error bars represent the Poisson errors ($N^{-1/2} / \ln 10$) in the number of binaries falling into each bin of separation.

At close separations, $\theta < 10"$, selection effects due to blending are dominant, and we are able to identify fewer and fewer binaries as the separation decreases. As discussed above, for separations larger than 10", both 2MASS and USNO, the sources of rNLTT, are able to resolve even very bright stars and, furthermore, our search strategy (§2) was implemented in such a way that we are confident of being free of selection effects as a function of separation (but see last paragraph in this same subsection). At the wide end, both distributions are well described by linear relations in this log-log plot, corresponding to power laws of the form $f(\theta) \propto \theta^{-\alpha}$. Furthermore, the slopes α of both wide distributions appear to be very similar.

In order to quantify this result, we fit both wide ends to the functional form $f(\theta) = A\theta^{-\alpha}$. Instead of fitting the binned data shown in Figure 9, a maximum likelihood approach permits to use each binary as an independent data point. The disk distribution is fitted for the range $1.4 \lesssim \log \theta \lesssim 2.7$ (from 25" to 500"), which includes 313 binaries, and yields $\alpha = 1.72 \pm 0.07$. The halo distribution is fitted for the range $0.74 \lesssim \log \theta \lesssim 2.95$ (from 5".5 to 900"), which includes 66 binaries, and yields $\alpha = 1.53 \pm 0.10$. Hence, the two slopes are consistent. The uncertainties in the slopes are determined analytically using equation (2.4) of Gould (1995).

Next, in order to obtain the binary frequency as a function of semimajor axis, distances to the binaries need to be adopted. For this, we first follow Figure 8a, and place all the disk and halo binaries at their median distances of 60 and 240 pc, respectively. The resulting distributions of projected semimajor axis are shown in Figure 10a, where the agreement between them can be clearly appreciated. Two things are particularly noteworthy. First, with the adopted distances, the two distributions match extremely well. The agreement between their normalizations is so good that the halo distribution at its wide end appears just as a smooth continuation of the trend of the disk binaries. Second, both binary distributions cut off exactly at the separations where we stopped searching for them, *not showing any clear sign of a break or turnover* up to physical separations of 0.1 pc and 1 pc, for the disk and halo samples respectively.

If, instead of placing the disk and halo samples at their median distances, we use the color-magnitude relations derived in §4.2 to assign individual distances to each of the bi-

naries, we obtain the distributions shown in Figure 10b.¹ Note that the distributions of binaries broaden, with some binaries going to populate the region of small semimajor axis. In addition, at the wide end, the disk distribution now extends to physical separations as large as the widest halo binaries. Nevertheless, the qualitative results are not changed and both distributions of binary fraction are the same within the errors.

Finally, it must be mentioned that the flattening of the distribution of disk binaries, occurring at $\theta \sim 10'' - 25''$, is a puzzle to us. It occurs well beyond the angular separation at which blending is an issue, and it has no counterpart in the angular distribution of halo binaries. We investigated the possibility that it was due to an excess of bright stars present in the disk sample, but introducing a cutoff in brightness did not remove it. Finally, using USNO-B we searched for all the non-NLTT CPM companions between $10''$ and $30''$ of NLTT stars and found not nearly enough numbers to account for this deficit. We discuss this further in §5.

4.4. Luminosity and Mass Ratios

The left hand panels of Figure 11 (a,b) show the magnitude difference (i.e., ratio of luminosities) between primaries and secondaries of disk and halo binaries as a function of the apparent magnitude of the primary in the V band. We include only wide ($\theta > 10''$) binaries in the disk diagram, while for the halo diagram we include binaries at all separations to increase the statistics. At any given brightness of the primary, there is a maximum observed ratio of luminosities, occurring when secondaries are near the magnitude limit of rNLTT ($V \sim 19$), which produces the upper envelope that limits the location of the binaries in these diagrams. Even in the absence of a magnitude limit, the existence of the hydrogen burning limit ($M \sim 0.08 M_{\odot}$) would set a very similar boundary in plots like these. In our case, at a mean distance of 60 pc, MS stars of this limiting magnitude have masses slightly above $0.1 M_{\odot}$, while subdwarfs of this limiting magnitude at a mean distance of 240 pc are of $0.2 M_{\odot}$. Due to this narrowing of the range of magnitude differences as the primary gets fainter and fainter, it would be misleading to construct a distribution of luminosity ratios that includes the entire sample of binaries. Instead, one should study the luminosity ratios as a function of the luminosity of the primary, i.e., the distribution of the luminosities of secondaries of all binaries in a small interval of primary brightness. To do this, we select the sections limited

¹In Figure 10b we show the actual counts in each bin of physical separation because, since selection effects operate naturally on angular rather than physical variables, its proper normalization is not a straightforward procedure.

by dashed vertical lines in Figure 11a,b. Inspection of the distribution of disk binaries in these regions suggest a nearly uniform distribution of magnitude differences all the way from zero (equal magnitudes) to the maximum allowed value (secondary at the magnitude limit). In the case of the halo, it is possible to recognize a slight preference for smaller magnitude differences, although the statistics are not as good as in the disk case.

These raw distributions are, however, still incomplete descriptions of the real situation, since they could possibly include selection biases. For example, at any given primary brightness, it is increasingly difficult to pick up the secondary as this gets fainter and fainter, hence biasing the resulting distribution towards equal luminosity components. To account for this we replot the distributions by normalizing the number of binaries in each bin with respect to the entire rNLTT catalog. To illustrate this normalization, consider a disk binary in the brightest of the three selected regions, i.e., its primary having a V magnitude between 7 and 9. Let's say $V_1 = 7.5$ and $V_2 = 12$. Then, the magnitude difference between this binary's components falls in the bin $4 < \Delta V < 6$ of the distribution we are building. It is at this point where, instead of just adding exactly one binary to this bin, we want to compare its secondary with all the stars in the catalog that could have fallen in this same bin. Hence, we count all the disk stars in rNLTT with V magnitude between $V_1+4 = 11.5$ and $V_1+6 = 13.5$, and use this number as the normalization for the binary in question. Finally, depending on whether the samples of binaries are considered complete or incomplete themselves, one can perform this normalization either considering or not the completeness of rNLTT as a function of magnitude. The completeness function has been well characterized by Gould (2003a) as part of his kinematic fit of halo parameters². The center panels of Figure 11 (c,d) show the distributions of luminosity ratios of disk and halo binaries normalized with respect to the raw rNLTT catalog, while the right-hand panels (11e,f) show the same distributions when correcting rNLTT for incompleteness. The single-star samples used for normalization are the secure disk and halo ones introduced in §4.1.

To transform to mass ratios, we first obtain absolute magnitudes using the CMRs found in §4.2, and then derive the masses from mass-luminosity (ML) relations. For the disk sample we use the empirical ML relations of Henry & McCarthy (1993), while for the halo sample we use a theoretical ML relation corresponding to a metal-poor isochrone of 10 Gyr. This isochrone was built with the Yale Evolutionary Code (Guenther et al. 1992), running standard stellar models in steps of $0.05 M_\odot$ and metallicity $[Fe/H] = -1.5$. The transformation from theoretical (M_{bol}, T_{eff}) quantities to broad-band magnitudes and colors is performed using the Lejeune, Cuisinier, & Buser (1997) model atmospheres.

²The completeness of rNLTT as a function of magnitude given in equation (10) of Gould (2003a) has a typo in its third segment, $V_{break} < V < 20$. The function should equal zero for $V = 20$.

The results for mass ratios are presented in Figure 12, where we use the same format as that of Figure 11 for the luminosity ratios. Again, the disk diagrams include only wide ($\theta > 10''$) binaries, and the halo diagrams include binaries at all separations to increase the statistics. Figures 12a,b show the mass ratio of each binary as a function of the mass of the primary. The vertical dashed lines indicate the regions chosen to compute the mass ratio distributions that are shown in the central and right-hand panels. In Figure 12a, it is possible to see a slight overconcentration of binaries that pile up to the right of $M_{\text{primary}} \sim 0.5 M_{\odot}$, which is due to a kink in the ML relation of Henry & McCarthy (1993) at that same point. Both *raw* (i.e., pre-normalized) distributions (Figures 12a,b) show preference for equal mass components. This is most evident in the case of halo binaries, but is also present in the disk binaries.

When normalized with respect to the entire catalog (Figures 12c,d without correcting for incompleteness, and Figures 12e,f including such correction), a systematic pattern develops. Except for the solid-line histograms in the halo case (Figures 12d,f), the first two or three bins in all the distributions reveal a monotonic decrease from equal-mass binaries towards systems of higher mass-ratio, which is the expected behavior given the preference for equal-luminosity components shown by Figure 11. However, after these first bins, all the normalized distributions are rising. This is not expected given the monotonic form of the distributions of luminosity-ratios, so is likely to be due to some selection effect present in the data.

5. Discussion

5.1. Power laws and limits on halo dark matter

The most important result of this work is the measurement of the distributions of angular separations and semimajor axes of disk and halo wide binaries in the solar neighborhood. We find that the distributions of angular separations are well described by single power laws over more than two decades of angular separation (Figs. 9 and 10). Furthermore, the power laws extend all the way out to the widest binaries in the samples, i.e., there is no evidence for a break in either distribution up to physical separations of 0.1 pc and 1 pc, for the disk and halo samples respectively.

These results have the potential to be very useful to impose constraints on the nature of Galactic dark matter, as the widest binaries, because of their small binding energies, are easier to disrupt by passing encounters with massive objects. For disk binaries, issues like the existence of molecular clouds and spiral arms, as well as the broad range of ages of the binaries themselves, complicate any modeling of the interaction of the binaries and their

environment. In the case of the Galactic halo, however, most of those complexities are not present, and the results are easier to interpret. A thorough investigation of the disruption of wide binaries is presented in a companion paper (Yoo, Chanamé, & Gould 2003), but a simple order-of-magnitude calculation serves to illustrate this point.

Let us consider a halo binary of mass m and semimajor axis a , and suppose a black hole of mass M with a velocity V relative to the binary passes by at a distance b from the closest component of the binary. In the tidal limit ($b \gg a$), and using the impulse approximation, the black hole induces a relative change of velocities between the components of the binary given by,

$$|\Delta \mathbf{v}_1 - \Delta \mathbf{v}_2| \equiv \Delta v_{12} = \frac{2Gm}{V} \left(\frac{1}{b} - \frac{1}{b+a} \right) \simeq \frac{2Gm}{bV} \frac{a}{b} \quad (3)$$

In order for this velocity change to disrupt the binary, we require

$$(\Delta v_{12})^2 \sim \frac{Gm}{a}. \quad (4)$$

In the tidal limit, binary disruption is dominated by the perturber with the closest approach, which impact parameter can be estimated from the rate equation $\pi b^2(\rho/M)VT = 1$, where ρ/M is the number density of black holes in the halo, and T is the binary's lifetime. Replacing b^2 in the condition for disruption, we obtain

$$a \sim \left(\frac{4\pi^2 G \rho^2 T^2}{m} \right)^{1/3} \sim 0.1 \text{ pc}, \quad (5)$$

where we have used $\rho \sim 0.009 M_\odot \text{ pc}^{-3}$, $T \sim 10 \text{ Gyr}$, and $m \sim 1 M_\odot$. This same estimate is obtained by Binney & Tremaine (1987) for the disruptive effect of molecular clouds on disk binaries. Since the distribution of separations for halo binaries (Fig 10) shows no signs of a break near $a \sim 0.1 \text{ pc}$, one can infer that, if the Galactic halo was entirely composed of black holes with a typical velocity of $V \sim 300 \text{ km s}^{-1}$, then these cannot be more massive than $M \sim \pi a^2 \rho V T \sim 10^3 M_\odot$.

5.2. Disk versus halo binaries

The second important aspect of this work is the comparison of the properties of binaries that belong to different Galactic populations, providing new insights on the early processes

of star formation in environments that are so radically different today. We find, in the first place, that the distributions of separations of wide binaries in the disk and halo of the Galaxy are consistent with each other, including both their slopes and normalizations. Then, as shown in Figure 11, there is also good agreement between disk and halo binaries regarding their distributions of luminosity ratios: both populations show an increasing number of binaries towards equal luminosity components. Finally, Figure 12 shows hints for a preference of equal-mass binaries for both the disk and the halo (as one would expect from the clear preference for equal luminosity components), but the unexpected behavior of the distributions at large mass ratios seems to indicate that low-mass stars are over represented in our samples of binaries with respect to the underlying rNLTT catalog. Nevertheless, although the possible presence of such selection effects complicate their interpretation, both disk and halo distributions of mass ratios are qualitatively similar.

All the above similarities between the two populations suggest that stars in the disk and halo of the Galaxy formed under similar conditions, kinematically cold enough to allow the formation of very wide binaries in both populations. Alternatively, if the star-forming conditions in the early disk and halo of the Galaxy were very different, one would be led to postulate the action of one or more mechanisms, yet to be discovered, that make the properties of today’s disk and halo wide binaries as similar as we find in the present work.

There is, however, one puzzling difference between the disk and the halo binaries that was already noted in §4.3. The distribution of angular separations of disk binaries (Fig 9) shows a peak at $\theta \sim 25''$, while no such feature is seen in the distribution of halo binaries. This peak also is not present in the G-dwarf sample of Duquennoy & Mayor (1991) or the M-dwarf sample of Fischer & Marcy (1992), although their statistics are substantially smaller than that of this work over the region of overlap. Let us suppose, for a moment, that the origin of the peak is some selection effect that has escaped our scrutiny. Then we can think of two possibilities. First, perhaps blending is a much worse problem than we estimated, and is removing binaries as wide as $20''$ from our disk sample. However, the distribution of halo binaries strongly suggests that our sample is essentially complete down to $\theta \sim 4''$, well below the $\theta = 10''$ separation that we conservatively adopt as a safe limit above which one can regard our sample as free of selection effects due to blending in the source catalogs. Hence, this strange selection effect would have to be removing more than a hundred disk binaries while at the same time leaving the halo binaries almost untouched. We regard this hypothesis as very unlikely. As a second possible explanation, one might think that the presence of very bright stars in the disk sample, which are mostly absent from the halo sample, is the source of this irregularity. To explore this possibility, we progressively remove from the sample of disk binaries those having bright components. We find that no magnitude cutoff is able to make the flattening disappear, and hence we also reject this second explanation.

In an additional effort to understand this feature, we use USNO-B to search the neighborhood of NLTT stars for non-NLTT CPM companions between $10''$ and $30''$ (of course, also restricted to the area of our survey, the intersection between POSS I and the 2MASS Second Incremental Release). This exercise has two advantages. First, it serves the immediate purpose of studying whether the flattening in the disk distribution of binaries is an artifact of the NLTT catalog. Second, since this search is restricted to a range of separations narrow enough to allow us to ascertain the reality of the candidates on a case-by-case basis (a rather painful task if we were to search the entire range of separations of this catalog), we also obtain an estimate of how many real binaries are being missed by restricting ourselves to NLTT stars.

From inspection of Figure 9 one can see that ~ 200 binaries between $10''$ and $30''$ are needed in order to make the disk distribution consistent with the power law derived for $\theta > 25''$. The search in USNO-B returned 58 candidate CPM companions, of which 31 turn out to be due to the diffraction spikes of bright NLTT stars, and 5 are USNO-B misidentifications of the NLTT star. Thus, we find 22 real non-NLTT CPM companions of NLTT stars in the range of separations between $10''$ and $30''$. The magnitude distribution of these stars is presented in Figure 13, where we compare it with that of the secondaries of disk binaries in our final sample. Most of the newly found CPM companions are indeed very faint, corresponding exactly with the secondaries we know we must be missing due to the declining NLTT completeness at these faint magnitudes (Gould 2003a). In conclusion, this search outside NLTT essentially added only those binaries already expected to be missing because of NLTT’s magnitude limit, and these account for only $\sim 10\%$ of the extra binaries needed to explain the flattening in the disk distribution as an artifact of NLTT.

We cannot think of any other obvious selection effect that could be responsible for this peak in the disk distribution of angular separations while at the same time not producing a similar feature in the corresponding distribution of halo binaries. In terms of actual semimajor axis, Figure 10 shows the flattening in the disk distribution occurring at $a \sim 1,500$ AU. Since the power law of the halo distribution does not probe too far inside this region of physical separation (there may be a hint that it goes to $a \sim 1,000$ AU, but this is already the region where blending begins to affect our completeness), we cannot determine whether the same feature is present or not in the distribution of halo semimajor axis.

5.3. Comparison to the samples of Ryan (1992) and Allen et al. (2000)

Selecting CPM pairs with RPMs indicative of halo stars, Ryan (1992) constructed a sample of 25 wide ($\theta > 10''$) halo binaries from NLTT. Of these 25, 2 are actually part

of triple systems and 10 are outside the intersection of POSS I and the 2MASS Second Incremental Release, leaving 13 CPM pairs inside the area of our survey. We indeed recover these 13 binaries, although 4 of them (with primaries NLTT 9308, 13320, 16468, and 54708) we classify as disk binaries, while a fifth one (NLTT 28236) is not included in our final samples because of a large proper-motion difference between its components. Recall that the selection and classification based on rNLTT data have several advantages with respect to that based on NLTT data alone, most notably, the availability of independent proper-motion measurements for the components as well as a larger color baseline (optical-infrared color). Hence, there is agreement in the classification of 8 of the 13 wide halo binaries common to our sample. Finally, Ryan (1992) does not attempt a study of the distribution of angular separations with this small sample, and focuses instead on a discussion of photometric parallaxes and the fraction of close companions to some of the CPM stars.

Allen et al. (2000) searched in NLTT for CPM companions of a sample of local high-velocity and metal-poor stars with Strömgren photometry. They compiled a total of 122 wide binaries ($a > 25$ AU) and, by computing their Galactic orbits along with their photometric metallicities, classified them as disk, thick disk, or halo stars. Since their underlying source for identifying binaries is the NLTT catalog, we compare their sample with that presented in this work and contrast our results. Note that, since Luyten intentionally recorded as identical the proper motions of the components of systems he regarded as binaries (this, despite the fact that he was in some cases able to measure their actual non-zero difference in proper motion), Allen et al. (2000) have no way to independently measure the proper-motion difference between the components and hence to identify and exclude false associations from their sample, as we do with our binaries in §2.

Of their 122 binaries, 55 match the conditions of our search (that is, stars inside the intersection of POSS I and the 2MASS Second Incremental Release), of which 37 are common to our final clean samples. Examination of these 37 common binaries in the RPM diagram of Figure 14 reveals that almost all of them have G-type primaries (compare the binaries in Fig. 14 with those randomly selected from our final samples and shown in Fig. 3). Of the remaining $55 - 37 = 18$ binaries, 4 are actually in our datasets but were rejected because of various reasons: one is actually a triple system, another includes a WD companion, and the other two have components with inconsistent positions on the RPM diagram (these last two pairs can be seen in Fig. 14 as the lines crossing the $\eta = 0$ boundary). This leaves 14 binaries in the Allen et al. (2000) sample that were not picked up by our search. However, all these 14 systems have angular separations smaller than $5''$, which is exactly the region where blending of the images of the two components limits our completeness. In conclusion, the Allen et al. (2000) sample supports our claim that we have recovered essentially all the CPM binaries with separations larger than $10''$.

While we classify our binaries as belonging to either the Galactic disk or halo on the basis of the RPM of the components (§3), Allen et al. (2000) use the complete space velocity of their stars (to compute Galactic orbits) and the metallicity estimate from Strömgren photometry to assign their binaries to a given population. Of the 37 binaries common to both works, there is perfect agreement in the classifications for all but 3 binaries. Given the fact that Allen et al. (2000) have more information available to classify their binaries, this agreement shows that our classification scheme based on RPM diagrams works very well. Regarding the 3 discrepant cases (HIP 25137, HIP 85378, and G85–17), they classify them as halo binaries, while we say disk. The space velocities of these 3 binaries would be consistent with either thick-disk or halo kinematics. The metallicities, $[Fe/H] \sim -0.6$, are however perfectly consistent with the thick-disk, but would lie at the high end of the halo metallicity distribution. Hence, we believe it would be appropriate to classify them as thick-disk stars. In any case, and despite these 3 discrepant cases, the agreement in the classification of the set of binaries common to both works is very good.

Although not directly mining the entire catalog for a complete sample of CPM binaries, the work of Allen et al. (2000) constitutes the most extensive attempt at studying NLTT binaries previous to the present work. One of their main conclusions is that the separations of wide binaries follow Oepik’s distribution ($f(\theta) \propto \theta^{-1}$), which does not agree with the power laws derived in this work. The reason for this disagreement is probably twofold. On the one hand, they do not take into account the problem of blending at close angular separations, which causes them to miss (just as we do in our own samples) binaries with faint secondaries that are just impossible to distinguish too close to a brighter primary. Second, they choose to visualize their data using cumulative distributions, which, in complicity with the first issue, are not as straightforward to interpret as the differential log-log distributions that we use in Figures 9 and 10.

In Figure 15 we compare the Allen et al. (2000) data with ours, both as cumulative distributions (upper panel) as well as in differential log-log form (lower panel). In the cumulative distributions we only compare binaries in the range $10''$ to $500''$, where we know the problems of blending are negligible and both samples should be essentially free of selection effects as a function of separation. Oepik’s law is represented by the straight dashed line joining the first and last data points, and it is immediately obvious that their sample (represented as crosses) does not follow it. Instead, their cumulative distribution for $10'' < \theta < 500''$ looks very similar to that of our sample of wide disk binaries (solid line), which was shown in §4.3 to follow a power law with slope of $\alpha = -1.72$, considerably steeper than Oepik’s distribution. Finally, the lower panel of Figure 15 shows that the differential log-log distributions of the entire Allen et al. (2000) sample (i.e., not restricted to $\theta > 10''$) and our sample of disk binaries are in almost perfect agreement for $\theta \gtrsim 25''$. Hence, one

can appreciate how much would the Allen et al. (2000) conclusions have changed if they had used differential rather than cumulative distributions to visualize their data.

6. Conclusions

We have compiled a catalog of wide binaries ($a \gtrsim 100$ AU) selected from among all the common proper motion (CPM) systems present in the rNLTT catalog, restricting the search to the area of the sky comprised by the intersection between POSS I and the 2MASS Second Incremental Release. With the help of the recently released USNO-B catalog, our search has been extended to most NLTT stars in this overlap region that were not initially recovered by rNLTT. Given that independent proper motions are available for essentially all the components of our CPM pairs, we impose a selection criterion based on the proper-motion difference as a function of angular separation ($\Delta\mu - \theta$ plane) to select good binary candidates. The selected sample is then classified with the aid of reduced proper motion (RPM) diagrams into disk and halo subsamples. The classification procedure also serves to identify unrelated pairs that were not rejected by the selection cut (mostly, unphysical pairs with disk and halo components at the same time). Disk binaries are searched up to angular separations of $500''$, and halo binaries up to $900''$. These correspond to semimajor axes of 0.1 pc and 1 pc, for the disk and halo samples respectively.

The final clean samples have 794 and 111 disk and halo binaries respectively, by far the largest dataset of wide binaries available to date. The subsets restricted to separations larger than $10''$, with 512 and 49 disk and halo binaries respectively, are essentially free of selection effects as a function of angular separation. Most of the stars in these binaries have spectral types between M0 and M5.

We compute the distributions of angular and physical separations of the final samples of disk and halo binaries (Figs. 9 and 10). Both distributions follow power laws of the form $dN/d\theta \propto \theta^{-\alpha}$, and we find $\alpha = 1.72 \pm 0.07$ and $\alpha = 1.53 \pm 0.10$ for the disk and halo respectively. Hence, the two slopes are consistent at the 1.6σ level. Furthermore, their normalizations are also consistent. We also compute the distributions of luminosity and mass ratios between primaries and secondaries (Figs. 11 and 12), and find that disk and halo binaries are also similar in these respects: both binary populations show a clear preference for equal-luminosity components, and a somewhat less clear (probably because of selection effects) preference for equal-mass components.

In light of all these similarities we conclude that, despite the fact that the disk and halo binaries belong to very different stellar populations today, they probably formed under

similar environmental conditions, kinematically cold enough to produce bound systems as wide as those reported here. At least as concerns binaries, the end result of the star-formation process on large scales seems to be independent of the metallicity of the environment.

We find that the distribution of disk binaries flattens in the region of $10'' - 25''$. Though unexpected, this feature has a high statistical significance, and occurs in a range of angular separation where selection effects due to blending are not at work. We have explored various scenarios that could hypothetically account for this flattening, even looking for more CPM companions outside NLTT, but nothing could remove it. Hence, we consider this flattening a real structure in the distribution of wide disk binaries. Since they are farther away than the disk sample, the halo binaries do not probe the same range of physical separation, and we therefore cannot explore whether the same structure is present or not in the halo distribution.

Finally, both disk and halo binaries show no evidence for a break or turnover in their distributions, smoothly extending all the way up to the limits of our search. Given that the widest binaries are easily disrupted by close encounters with large mass concentrations, these results provide the opportunity to place limits on the nature and properties of dark matter in the Galactic halo. We carry out a detailed investigation of these limits in Yoo, Chanamé, & Gould (2003).

This work was supported in part by grant AST 02-01266 from the NSF and by JPL contract 1226901.

A. Description of Catalog

The catalog is arranged so that each line describes one pair of stars. The data for each pair is grouped in six sections, 1) identifiers, 2) positions, 3) proper motions, 4) photometry, 5) 3-digit source codes, 6) binary information. Sections 1 to 5 give the corresponding information for the two stars immediately next to each other. That is, section 3, for example, includes 4 entries: 2 for the two components of the proper motion of the first star, and 2 for the components of the second star.

The ordering of the two stars in each pair follows the corresponding NLTT numbers in ascending order, and from this point on, the first star in each pair will be labeled A, and the second will be labeled B. Section 1 contains two entries: 1) NLTT(A), 2) NLTT(B). Section 2 contains 4 entries: 3) α (A), 4) δ (A), 5) α (B), 6) δ (B), where all coordinates are epoch and equinox 2000. Section 3 contains: 7) μ_α (A), 8) μ_δ (A), 9) μ_α (B), 10) μ_δ (B), in units of arcsec yr^{-1} . Section 4 contains the photometry: 11) V_A , 12) $(V - J)_A$, 13) V_B , 14) $(V - J)_B$.

Section 5 contains two entries: 15) 3-digit source code for A, 16) 3-digit source code for B.

The three digits of the source code are the same as those introduced in Salim & Gould (2003). As summarized there, the digits refer to the sources of the position, proper motion, and V photometry. 1 = Hipparcos, 2 = Tycho-2, 3 = Tycho Double Star Catalog, 4 = Starnet, 5 = USNO/2MASS, 6 = NLTT, 7 = USNO (for position) or common proper motion companion (for proper motion). More specifically, “555” means 2MASS based position, USNO based V photometry, and USNO/2MASS based proper motion. For additional details see Salim & Gould (2003). For the purposes of this catalog, we introduce two more digits for coding: 0 = the star is not recovered by rNLTT, and the position is the same as that of the rNLTT companion, 8 = USNO-B.

Finally, section 6 of each catalog line contains the binary information: 17) classification code for the common proper-motion pair, 18) magnitude of the vector proper-motion difference between the components (arcsec yr^{-1}), 19) angular separation (arcsec), 20) position angle of B with respect to A (degrees), 21) rNLTT binarity indicator, 22) indicates whether the pair is (1) or is not (0) in the sample of Allen et al. (2000). The classification code indicates: 1 = disk binary, 2 = halo binary, 3 = at least one component is a white dwarf, 4 = rejected because of uncertain classification, 5 = rejected because of components have inconsistent RPM positions, 6 = rejected because of a large proper-motion difference or it is beyond the limits of our search, 7) rejected because one component was not found in any available sources. Regarding the binarity indicator: 0 = both NLTT stars are not present in rNLTT, 1 = NLTT regards it as a binary but rNLTT did not recover one of the components, 2 = NLTT regards it as a binary and both components are present in rNLTT, 3 = NLTT does not regard this as a binary.

The catalog in ascii format can be retrieved from
http://www.astronomy.ohio-state.edu/~gould/rNLTT_binaries/binaries.dat.gz.

The Fortran format statement for the catalog record is:
(i5,i6,4f11.6,4f8.4,4f6.2,1x,3i1,1x,3i1,i2,f8.4,f7.1,f6.1,2i2)

B. New halo stars with Hipparcos parallaxes

In Table 2 we present 11 halo binaries for which one of the components is an Hipparcos star, and hence, their companions become new halo stars with available parallaxes. Of the 11 binaries, only 5 have accurate parallaxes, and these correspond to the first entries of the table.

The entries in Table 2 are as follows: 1) Hipparcos ID, 2) NLTT number of the Hipparcos star, 3) NLTT number of the companion of the Hipparcos star (i.e., the new halo star with parallax). From this point, the Hipparcos star is labeled A, and the companion is labeled B. The next entries are: 4) angular separation (arcsec), 5) position angle of B with respect to A, 6) $M_V(A)$, 7) V_A , 8) $(V - J)_A$, 9) $M_V(B)$, 10) V_B , 11) $(V - J)_B$, 12) parallax (mas), 13) parallax uncertainty (mas). A superscript 'a' indicates three binaries where one of the stars straddle the boundary between disk and halo stars, and should not be taken as halo binaries with full confidence.

REFERENCES

Allen, C., Poveda, A., & Herrera, M. A. 2000, *A&A*, 356, 529

Bahcall, J.N. & Soneira, R.M. 1981, *ApJ*, 246, 122

Binney, J., & Tremaine, S. 1987, in *Galactic Dynamics*, Princeton University Press

Bouvier, J., Rigaut, F., & Nadeau, D. 1997, *A&A*, 323, 139

Close, L.M., Richer, H.B., & Crabtree, D.R. 1990, *AJ*, 100, 1968

Duchêne, G. 1999, *A&A*, 341, 547

Duquennoy, A., & Mayor, M. 1991, *A&A*, 248, 485

Finlator, K., et al. 2000, *AJ*, 120, 2615

Fischer, D. A., & Marcy, G. W. 1992, *ApJ*, 396, 178

Garnavich, P.M. 1988, *ApJ*, 335, L47

Garnavich, P.M. 1991, PhD Thesis, (St. Louis:Washington University)

Ghez, A. M., Neugebauer, G., & Matthews, K. 1993, *AJ*, 106, 2005

Ghez, A. M., McCarthy, D. W., Patience, J. L., & Beck, T. L. 1997, *ApJ*, 481, 378

Gizis, J.E. 1997, *AJ*, 113, 806

Gizis, J. E., Monet, D. G., Reid, I. N., Kirkpatrick, J. D., Liebert, J., & Williams, R. J. 2000, *AJ*, 120, 1085

Gould, A. 1995, *ApJ*, 440, 510

Gould, A., Bahcall, J.N., Maoz, D., & Yanny, B. 1995, *ApJ*, 441, 200

Gould, A., & Salim, S. 2003, *ApJ*, 582, 1001

Gould, A. 2003a, *ApJ*, 583, 765

Gould, A. 2003b, *AJ*, in press

Guenther, D. B., Demarque, P., Kim, Y.-C., & Pinsonneault, M. H. 1992, *ApJ*, 387, 372

Henry, T.J., & McCarthy, D.W. 1993, *AJ*, 106, 773

Høg, E. et al. 2000, A&A, 355, L27.

Latham, D.W., Tonry, J., Bahcall, J.N., Soneira, R.M., & Schechter, P. 1984, ApJ, 281, L41

Latham, D. W., Stefanik, R. P., Torres, G., Davis, R. J., Mazeh, T., Carney, B. W., Laird, J. B., & Morse, J. A. 2002, AJ, 124, 1144

Leinert, C., Zinnecker, H., Weitzel, N., Christou, J., Ridgway, S. T., Jameson, R., Haas, M., & Lenzen, R. 1993, A&A, 278, 129

Lejeune, T., Cuisinier, F., & Buser, R. 1997, A&AS, 125, 229

Luyten, W. J. 1979, 1980, New Luyten Catalogue of Stars with Proper Motions Larger than Two Tents of an Arcsecond (Minneapolis: University of Minnesota Press)

Luyten, W. J. & Hughes, H. S. 1980, Proper-Motion Survey with the Forty-Eight Inch Schmidt Telescope. LV. First Supplement to the NLTT Catalogue (Minneapolis: University of Minnesota)

Monet, D. G., et al. 1992, AJ, 103, 638

Monet, D. G. 1996, American Astronomical Society Meeting, 188, 5404.

Monet, D. G. 1998, American Astronomical Society Meeting, 193, 112003

Monet, D.G. 2002, AJ, 125, 984

Patience, J., Ghez, A. M., Reid, I. N., Weinberger, A. J., & Matthews, K. 1998, AJ, 115, 1972

Patience, J., Ghez, A. M., Reid, I. N., & Matthews, K. 2002, AJ, 123, 1570

Petr, M. G., Coude Du Foresto, V., Beckwith, S. V. W., Richichi, A., & McCaughrean, M. J. 1998, ApJ, 500, 825

Prosser, C. F., Stauffer, J. R., Hartmann, L., Soderblom, D. R., Jones, B. F., Werner, M. W., & McCaughrean, M. J. 1994, ApJ, 421, 517

Reid, I.N. 1991, AJ, 102, 1428

Ryan, S. G. 1992, AJ, 104, 1144

Salim, S., & Gould, A. 2002, ApJ, 575, L83

Salim, S., & Gould, A. 2003, ApJ, 582, 1011

Scally, A., Clarke, C., & McCaughrean, M. J. 1999, MNRAS, 306, 253

Simon, M. et al. 1995, ApJ, 443, 625

Skrutskie, M. F. et al. 1997, in The Impact of Large-Scale Near-IR Sky Survey, ed. F. Garzon et al (Kluwer: Dordrecht), p. 187

Wasserman, I. & Weinberg, M.D. 1989, ApJ, 382, 149

Weistropp, D. 1972, AJ, 77, 366

White, R. J. & Ghez, A. M. 2001, ApJ, 556, 265

Yoo, J., Chanamé, J., & Gould, A. 2003, submitted

Zheng, Z., Flynn, C., Gould, A., Bahcall, J., & Salim, S. 2001, ApJ, 555, 393

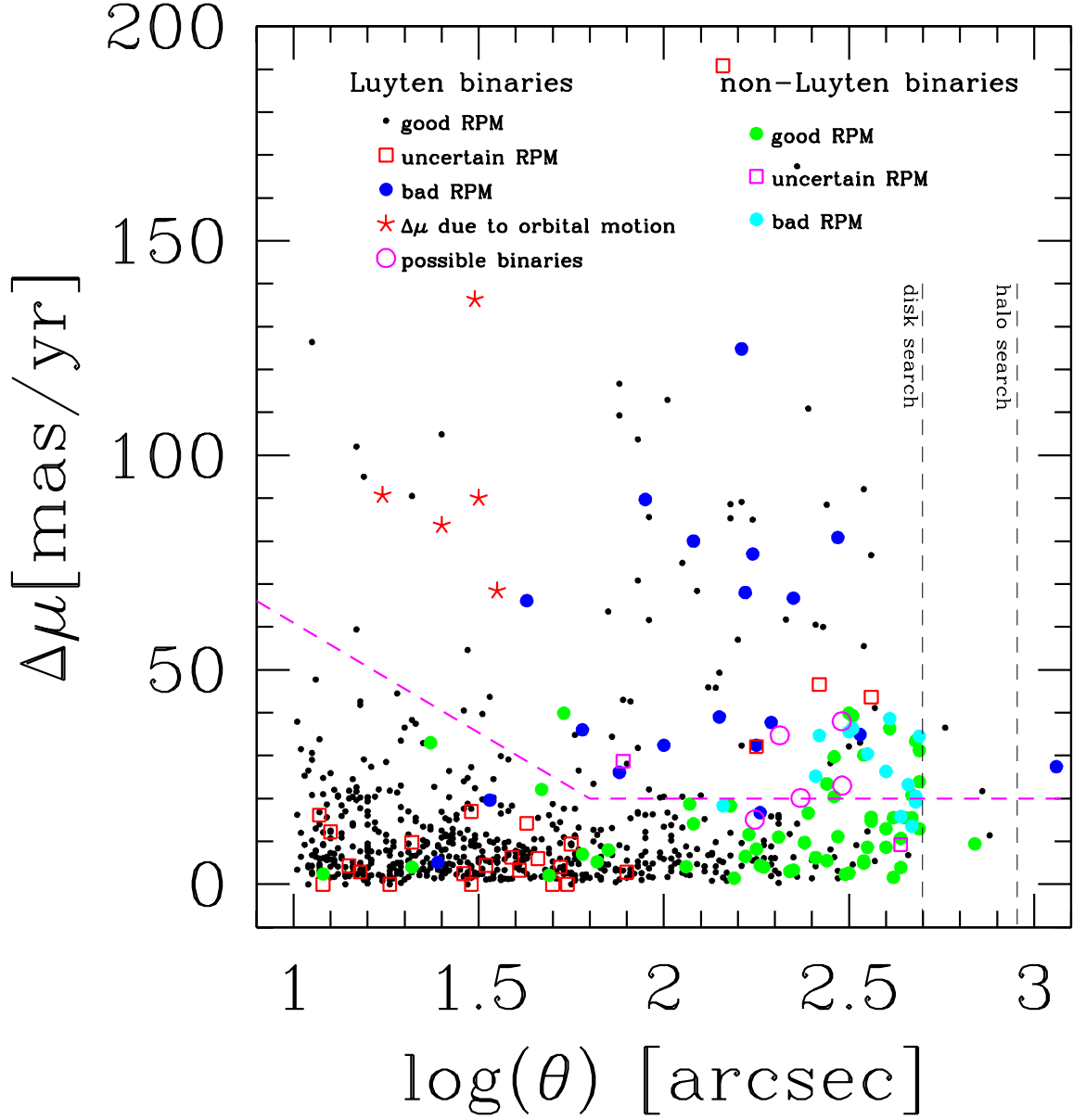


Fig. 1.— Vector proper-motion difference versus angular separation for the CPM systems with $\theta > 10''$. The dashed magenta line delineates our selection criteria for this “wide subsample”: CPM pairs below this limit are automatically accepted as candidate binaries for their subsequent classification. CPM pairs with proper-motion differences above the cutoff but inside $50''$ were individually investigated. Red stars indicate those whose large proper-motion difference is explained by significant orbital motions, and are accepted as good candidates for classification. The various colors and symbols encode the binaries as being genuine, of uncertain type, or bad (i.e., unrelated pairs), for both Luyten and non-Luyten classes, after they were subject to the classification procedure. Magenta circles indicate pairs that Luyten believed “might be” binaries. The dashed vertical lines indicate the upper limits of the search for disk and halo binaries.

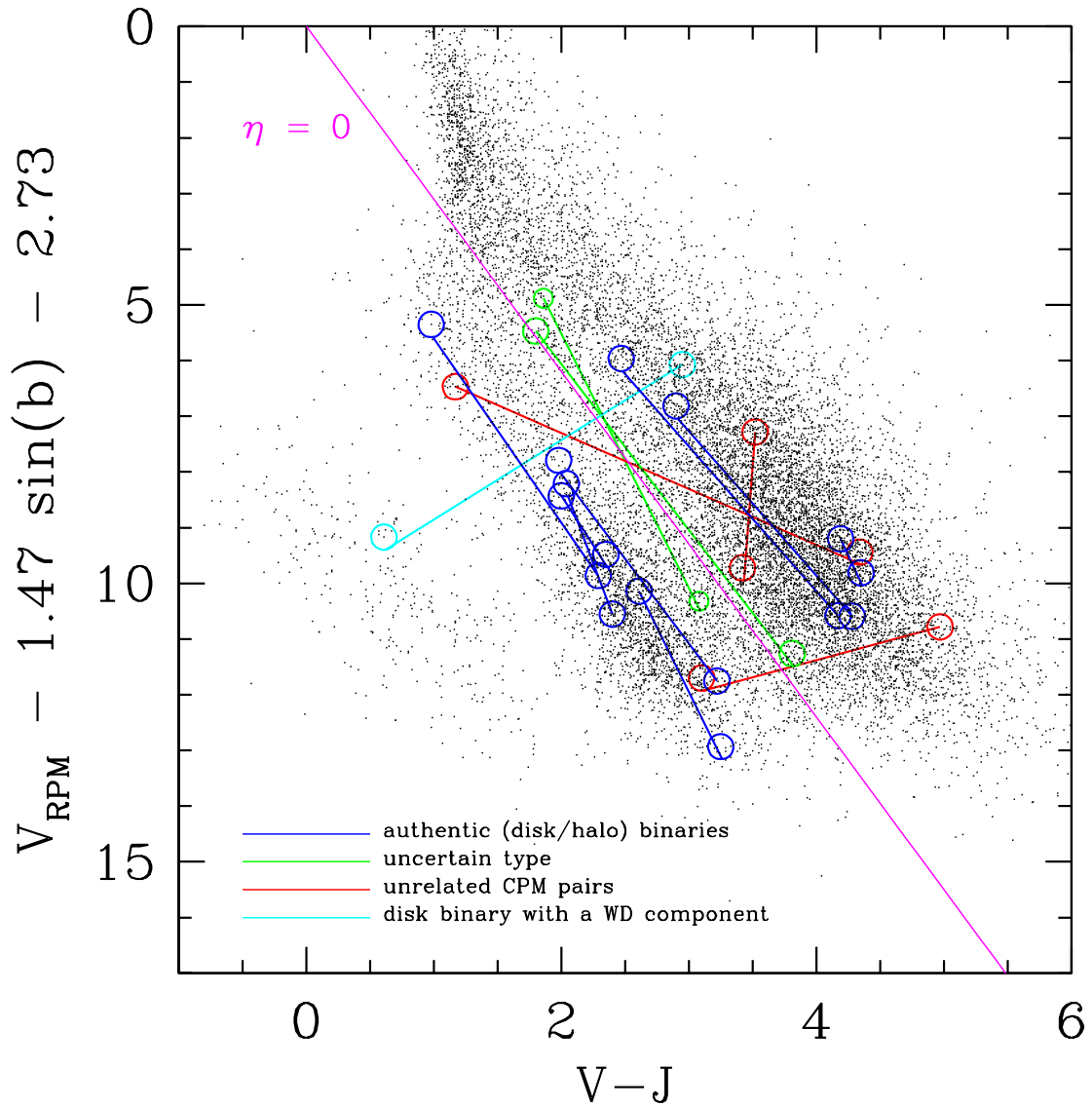


Fig. 2.— RPM diagram adjusted for Galactic latitude b clearly separating MS, SD, and WD tracks, with $\eta = 0$ (magenta line) being our formal MS/SD discriminator. A few representative examples of how this diagram is used to classify binaries are shown by pairs of circles connected by a line: genuine pairs, whether disk or halo (blue); probably genuine but unclassifiable pairs (green); optical pairs not physically associated (red); MS-WD pair (cyan). Note that pairs are also regarded as unphysical when the line connecting them is far from parallel to either the MS or SD track.

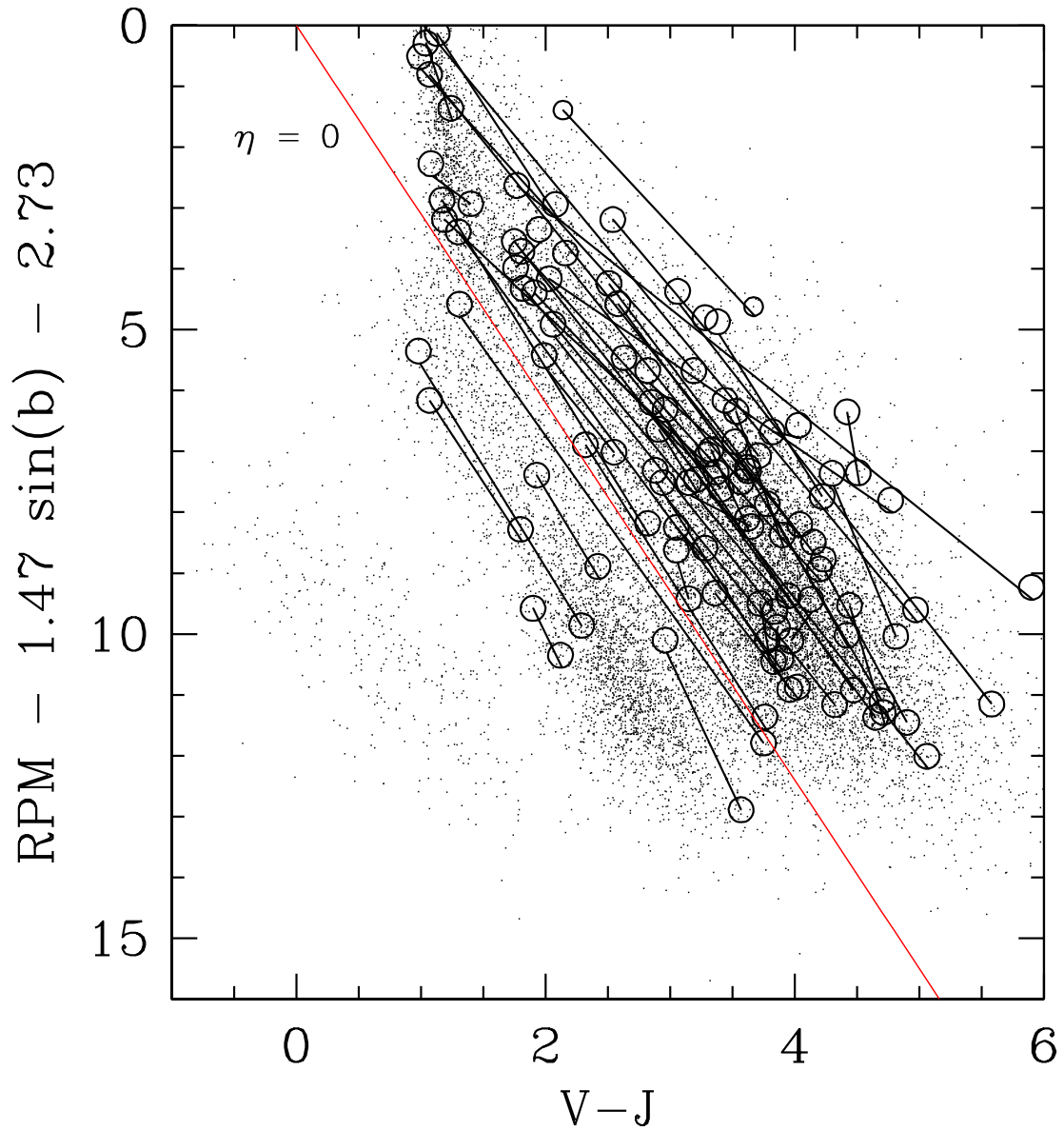


Fig. 3.— Graphical representation of $\sim 10\%$ of our binaries, randomly selected from the final clean wide sample ($\theta > 10''$). Note how real binaries have their components lying on the same isochrone, i.e., the line connecting them being approximately parallel to either the MS or SD track.

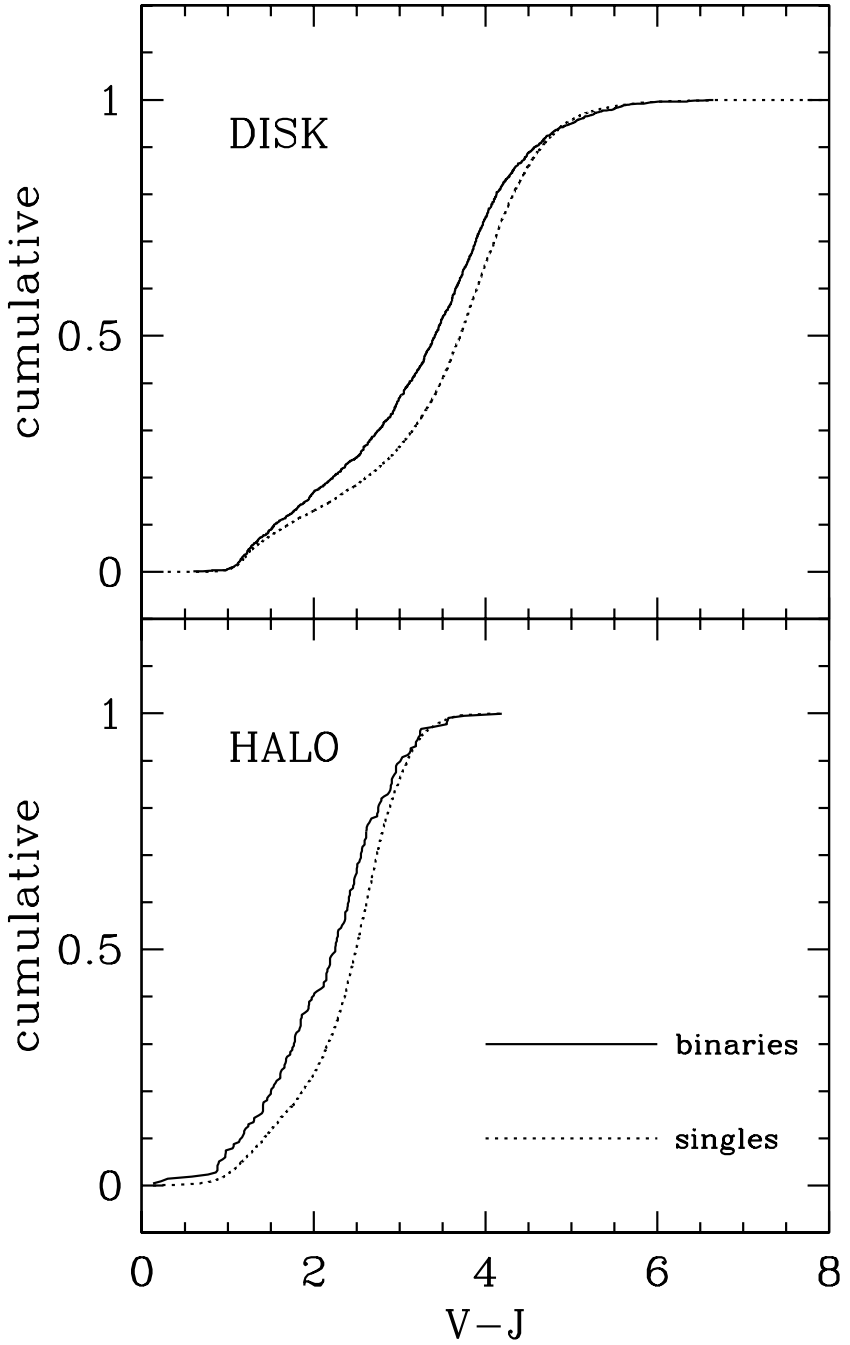


Fig. 4.— Cumulative color distribution of the stars in binaries compared to that of the entire rNLTT catalog, for the disk and halo populations separately. Due to the magnitude-limited nature of the rNLTT catalog, the companions of bright stars are preferentially selected in comparison to those of fainter ones, causing both samples of binaries to have larger fractions of blue (i.e., bright) stars than the catalog as a whole.

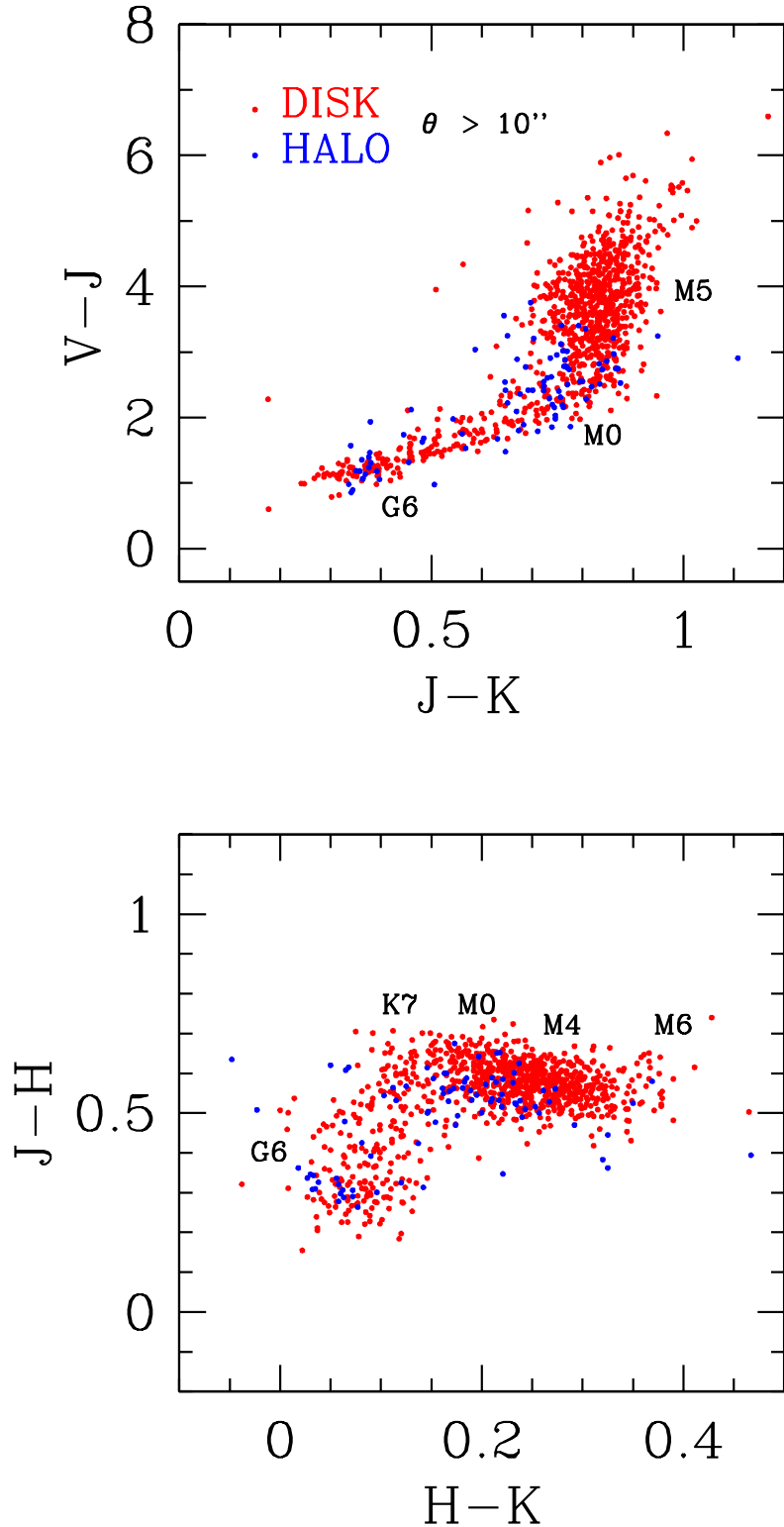


Fig. 5.— Color-color diagrams for all stars in the wide ($\theta > 10''$) sample, showing the approximate location of representative types of dwarf stars. Most of the stars in our binaries are of types M0 to M5.

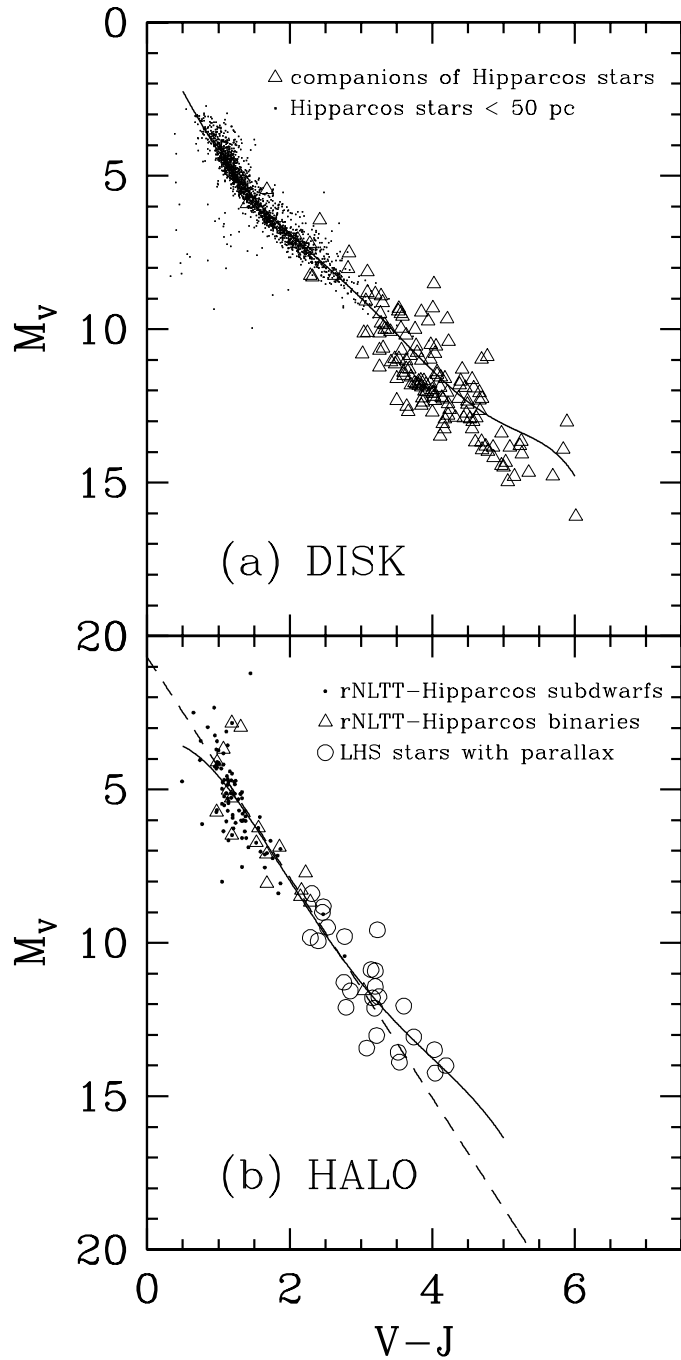


Fig. 6.— Color-magnitude diagrams of the parallax samples used in the determination of color-magnitude relations. (a) Disk parallax sample: small dots are all the Hipparcos stars within 50 pc of the Sun in the color range of interest. Open triangles represent all the companions of stars in our disk sample that have an Hipparcos parallax. (b) Halo parallax sample: small dots are all subdwarfs present in rNLTT with Hipparcos parallaxes. Open triangles are all the rNLTT stars in binaries that have one component with an Hipparcos parallax. Open circles are subdwarfs with parallaxes from Gizis (1997) and Monet et al. (1992). The solid lines are the polynomial fits to these data. The dashed line in the halo diagram is the linear fit from the kinematic analysis of Gould (2003a).

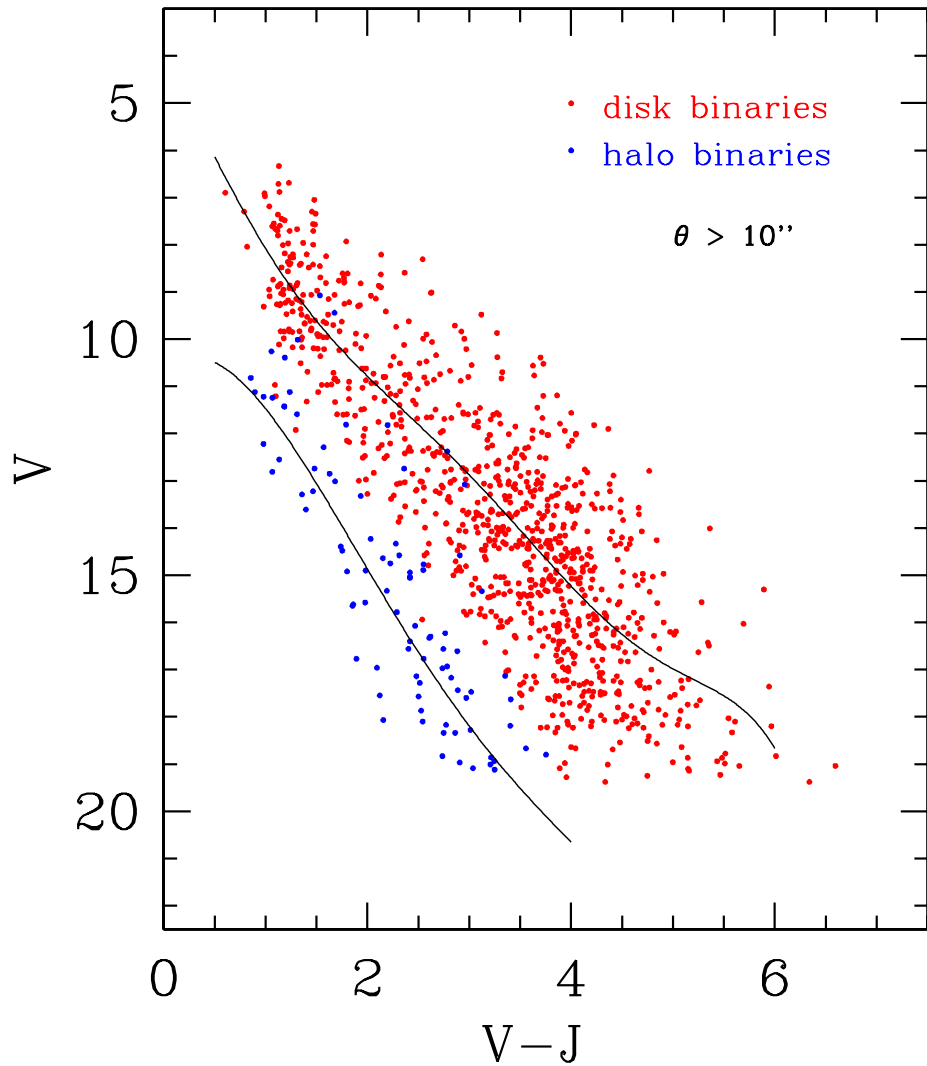


Fig. 7.— Color-magnitude diagram of the disk and halo samples of wide ($\theta > 10''$) binaries that satisfactorily passed the selection and classification procedures. The solid lines are the color-magnitude relations obtained from the parallax samples discussed in §4.2, and placed at distances of 60 and 240 pc, for the disk and halo binaries respectively.

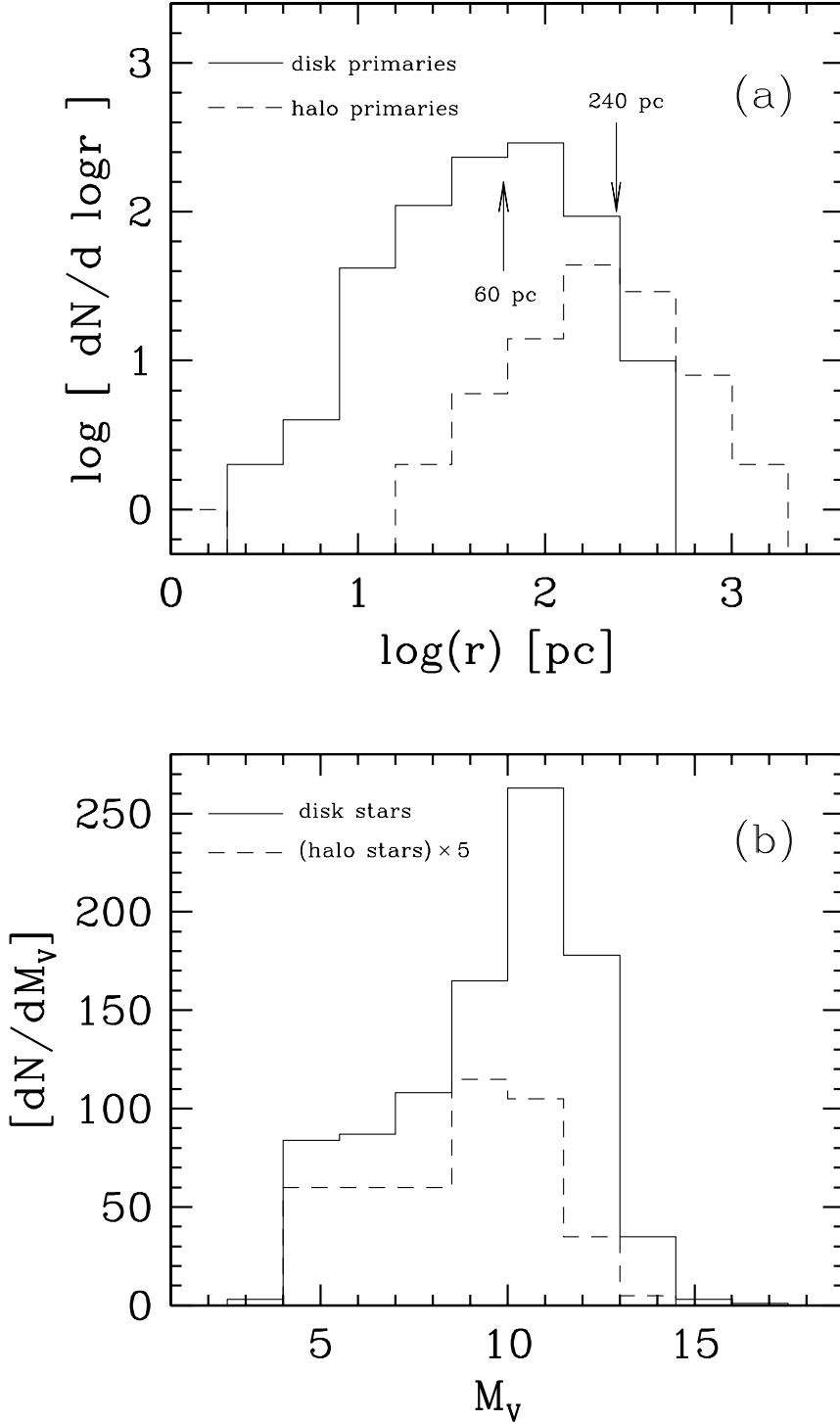


Fig. 8.— (a) Distance distribution of all the disk and halo primaries, as obtained with the color-magnitude relations found in §4.2. Both close and wide subsamples are included. From these distributions, average distances of 60 and 240 pc are adopted for the disk and halo samples, respectively. (b) V -band luminosity functions for stars in disk and halo wide ($\theta > 10''$) binaries, including primaries and secondaries, as obtained from the color-magnitude relations of §4.2. The locations of the peaks of the disk and halo luminosity functions are consistent with those found for solar neighborhood M dwarfs and subdwarfs, respectively.

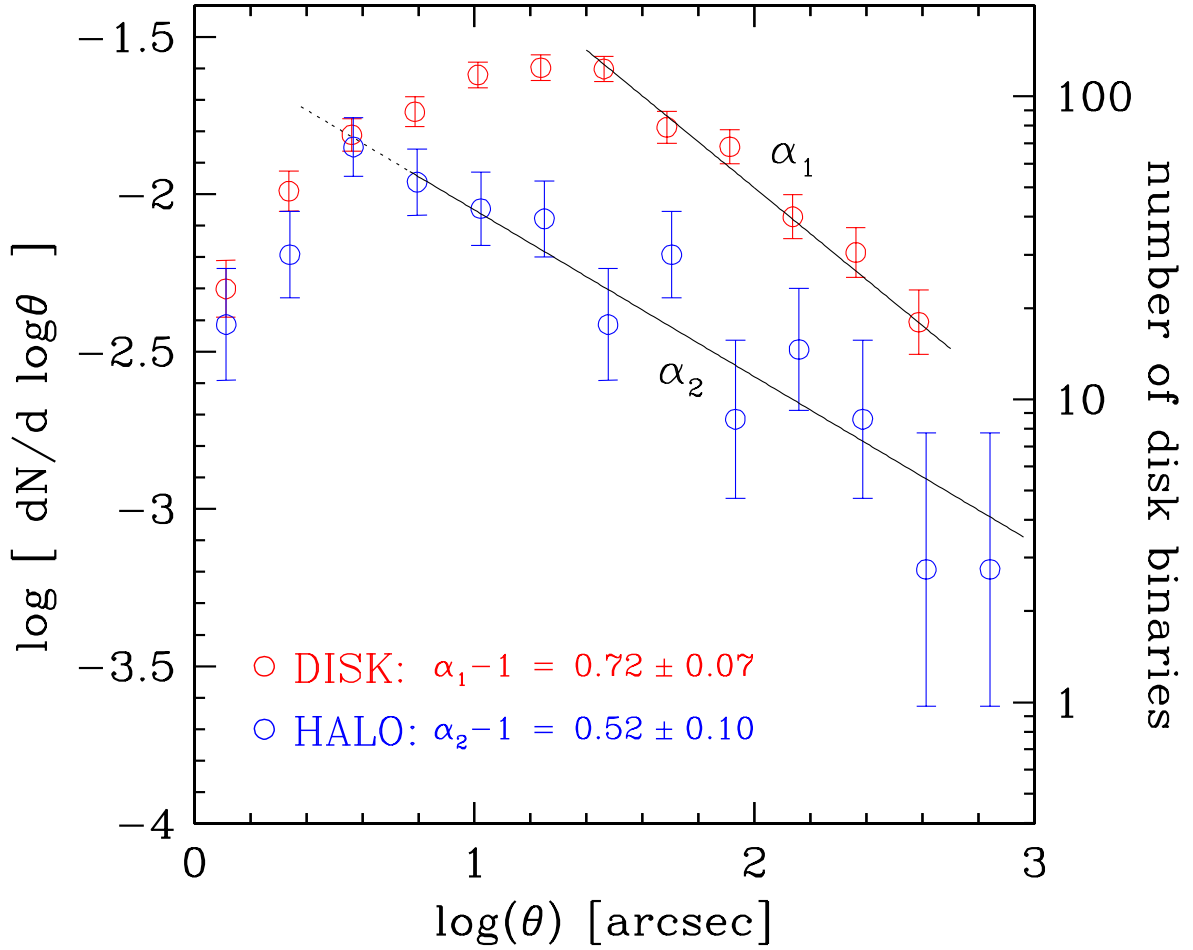


Fig. 9.— Distribution of angular separations for the final clean samples of disk and halo binaries. The normalizations are, respectively, with respect to all the disk and halo stars in the underlying rNLTT catalog. The scale of the right-hand vertical axis indicates the actual number of binaries in each bin of angular separation, and refers only to the disk distribution. The error bars represent Poisson uncertainties. The solid lines are the power-law fits obtained in §4.3, and are limited to the range of separations used in these fits. The dashed extension of the halo fit at the close end stresses the fact that the same power law still holds to separations even smaller than the those used in the fit. Note the flattening of the disk distribution between $10'' - 25''$, which has high statistical significance and occurs well outside the region of image blending (see §4.3 and §5.2).

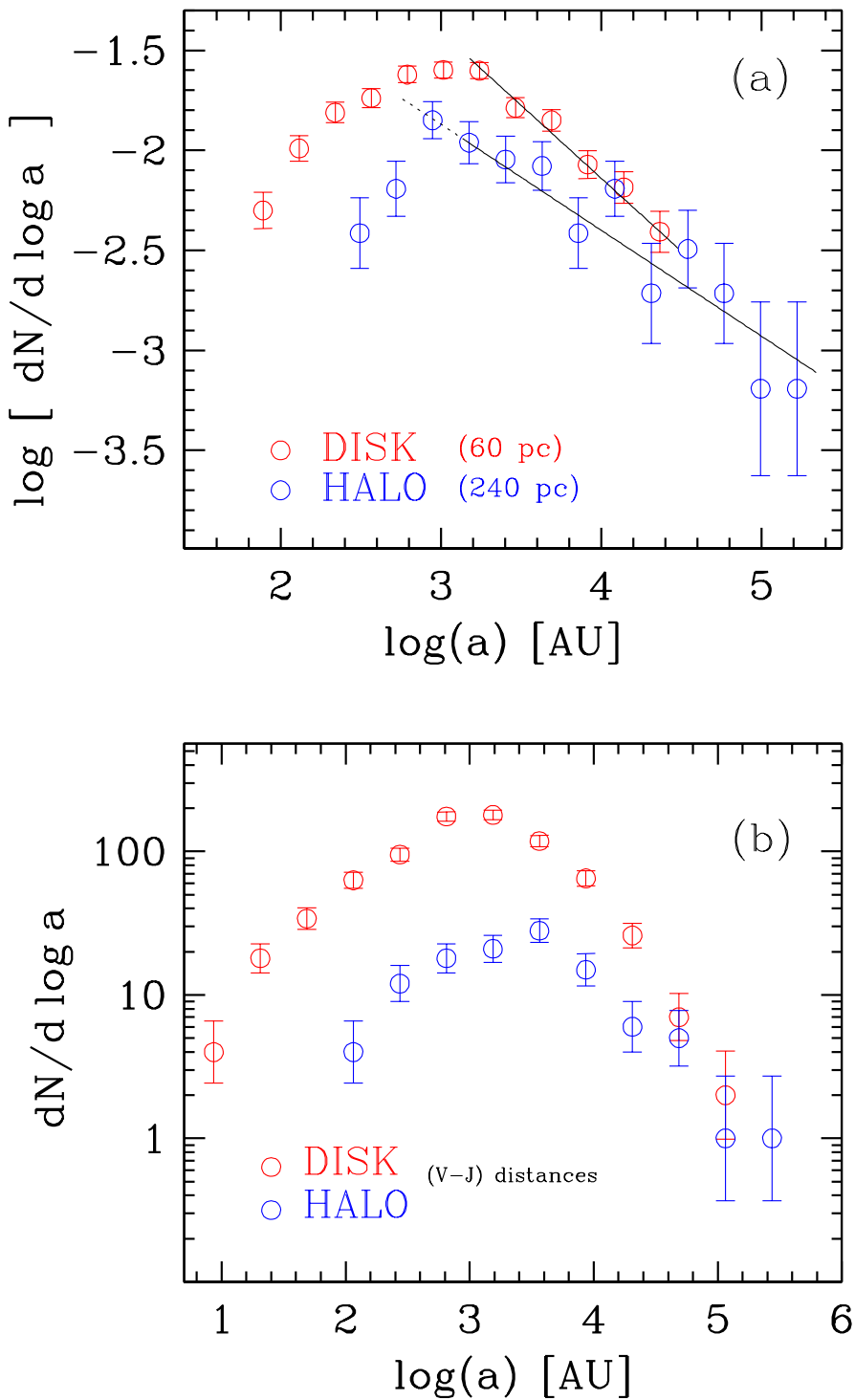


Fig. 10.— Distributions of physical projected separations for the final clean samples of disk and halo binaries, (a) using the average distances found in Fig. 8a for the disk and halo samples, and (b) using the individual distances to each of the binaries as obtained from the color-magnitude relations of Figs. 6 and 7. In (a) the normalizations relative to the entire rNLTT catalog have been preserved, while in (b) the actual counts, referring only to the disk binaries, are shown.

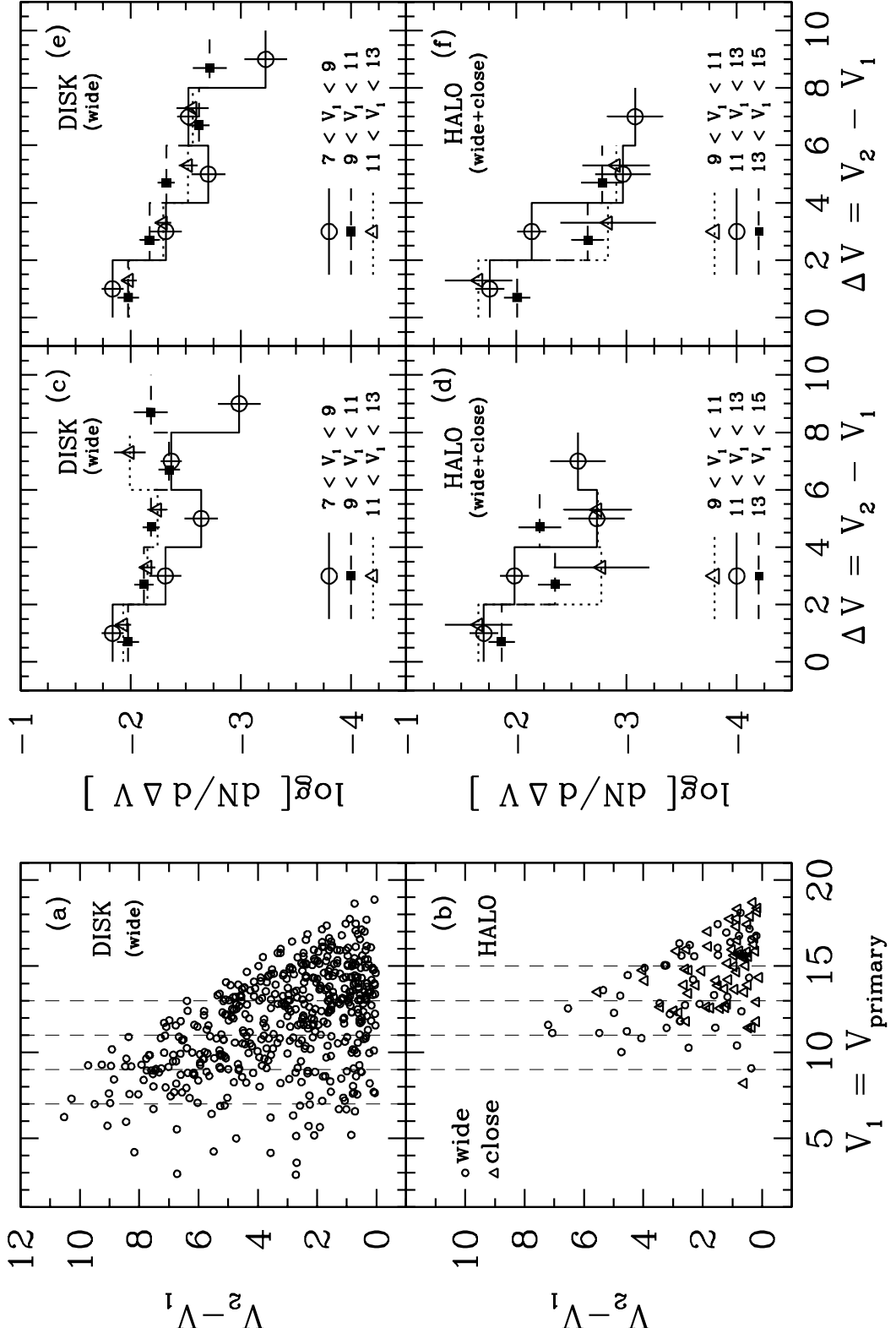


Fig. 11.— Distributions of luminosity ratios. (a,b) Magnitude difference between primaries and secondaries of disk and halo binaries as a function of the V -band magnitudes of the primaries. Only wide ($\theta > 10''$) binaries are included in the disk diagram, while binaries at all separations are included in the halo diagram. Note the magnitude limit of the rNLTT catalog as evidenced by the sharp upper envelope limiting the location of the points in these diagrams. The dashed vertical lines indicate the regions chosen to measure the distributions

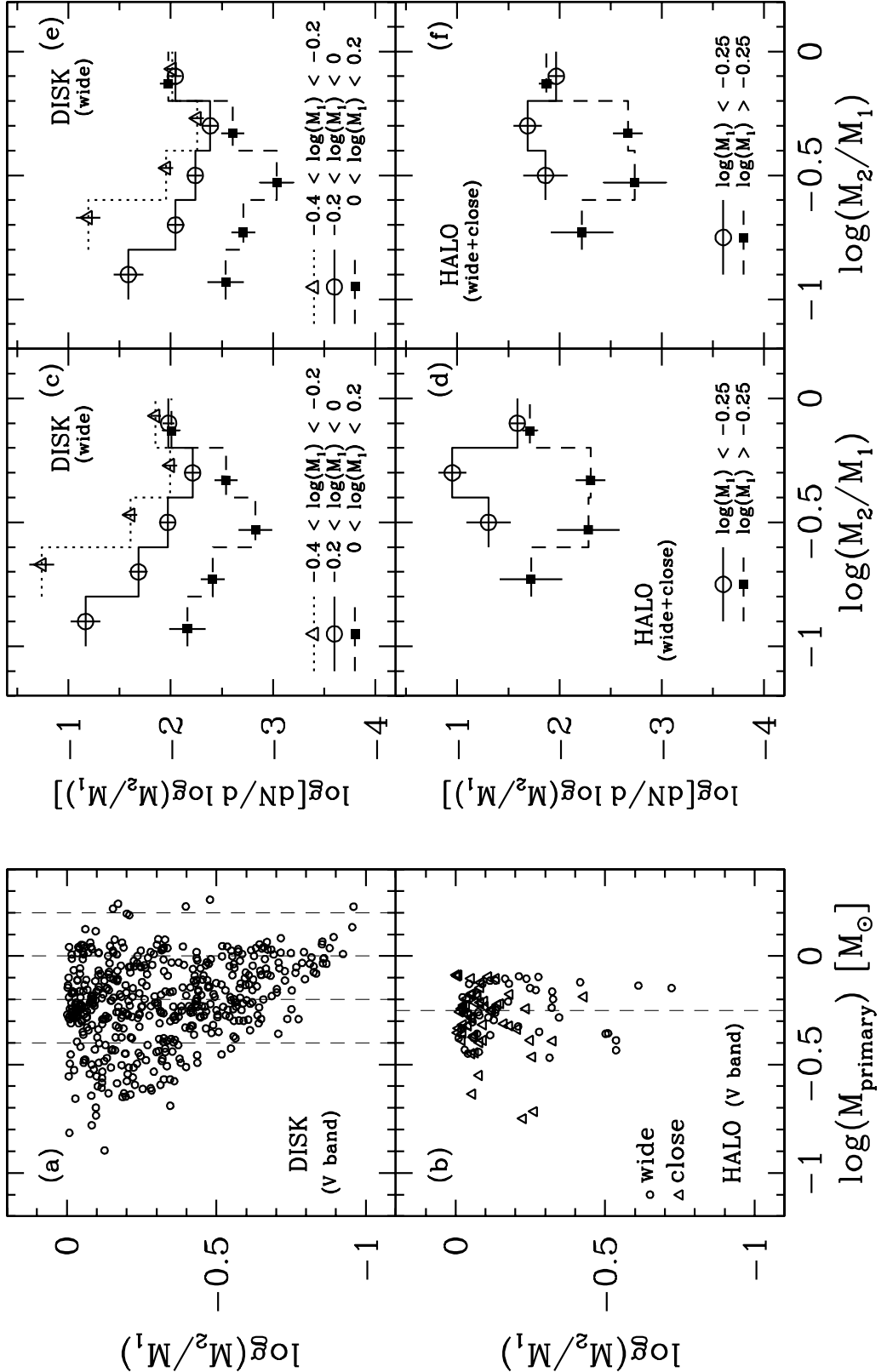


Fig. 12.— Distributions of mass ratios. (a,b) Ratio of the mass of secondaries to that of their primaries as function of primary's mass. Only wide ($\theta > 10''$) binaries are included in the disk diagram, while binaries at all separations are included in the halo diagram. The dashed vertical lines indicate the regions chosen to measure the distributions shown in the next panels. (c,d) Distributions of mass ratios for the ranges of primary mass selected in (a) and (b) and indicated by the dashed lines in the NTT sample ($\theta > 10''$ for the disk).

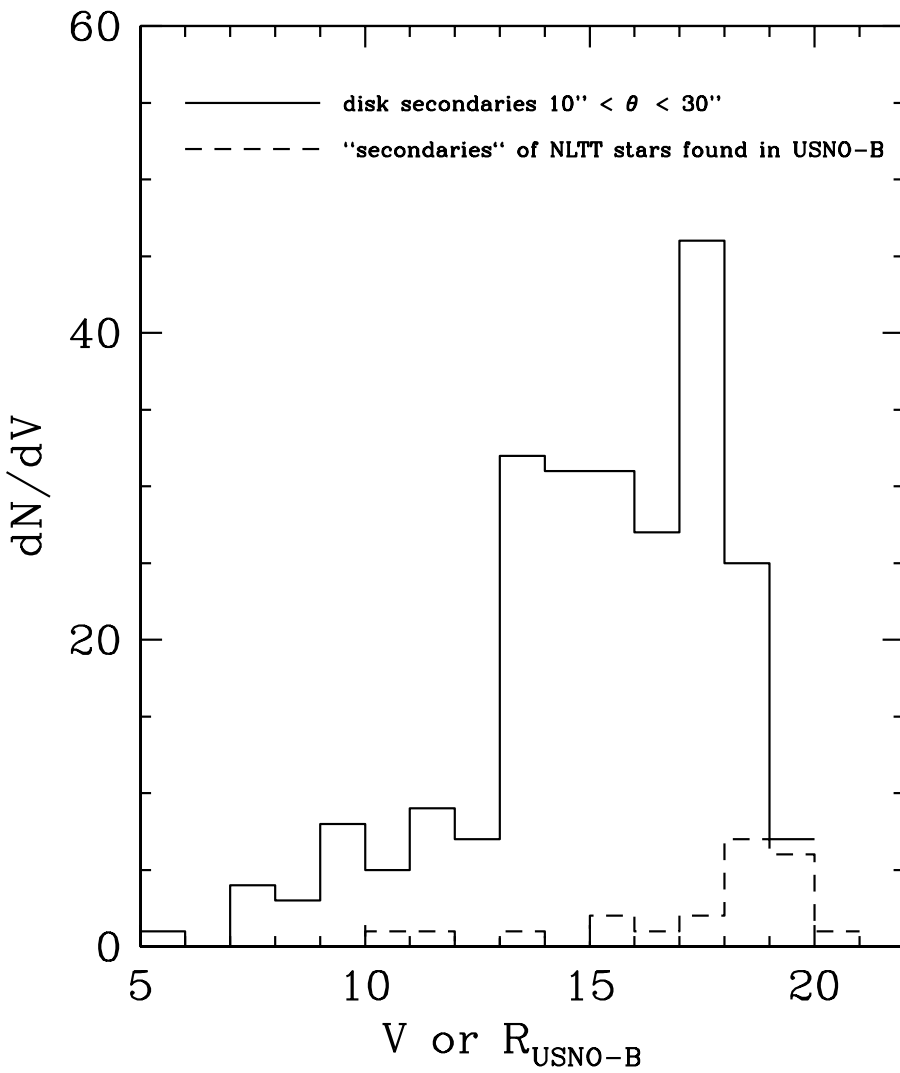


Fig. 13.— Search in USNO-B for non-NLTT CPM companions with separations $10'' < \theta < 30''$ from NLTT stars. Shown here is the distribution of USNO-B R magnitudes of the stars found (dashed histogram), in comparison to the distribution of V -band magnitudes of all the secondaries of disk binaries in our sample (solid histogram). The majority of the new CPM companions are very faint, consistent with the type of secondaries expected to be missing due to the NLTT catalog magnitude limit.

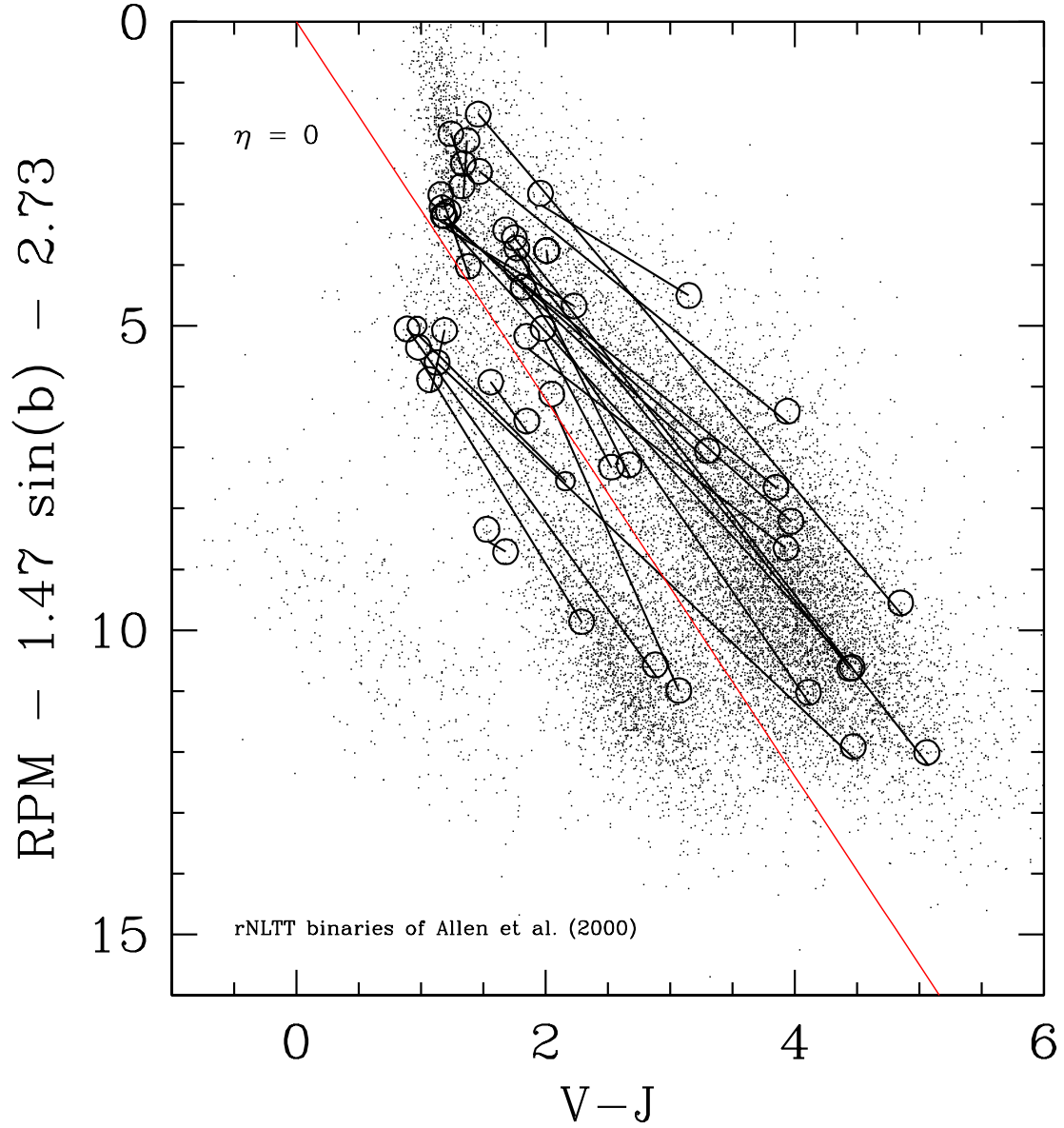


Fig. 14.— Reduced proper-motion diagram of all the binaries common to the work of Allen et al. (2000) and the present one. Comparison with the RPM diagram of Fig. 3 shows that almost all of the binaries in Allen et al. (2000) have G-type primaries. Note the two unphysical disk-halo pairs, with the lines connecting their components crossing the disk/halo boundary ($\eta = 0$). Six of the 37 binaries in common cannot be plotted here because one or both components do not have *J*-band measurements available.

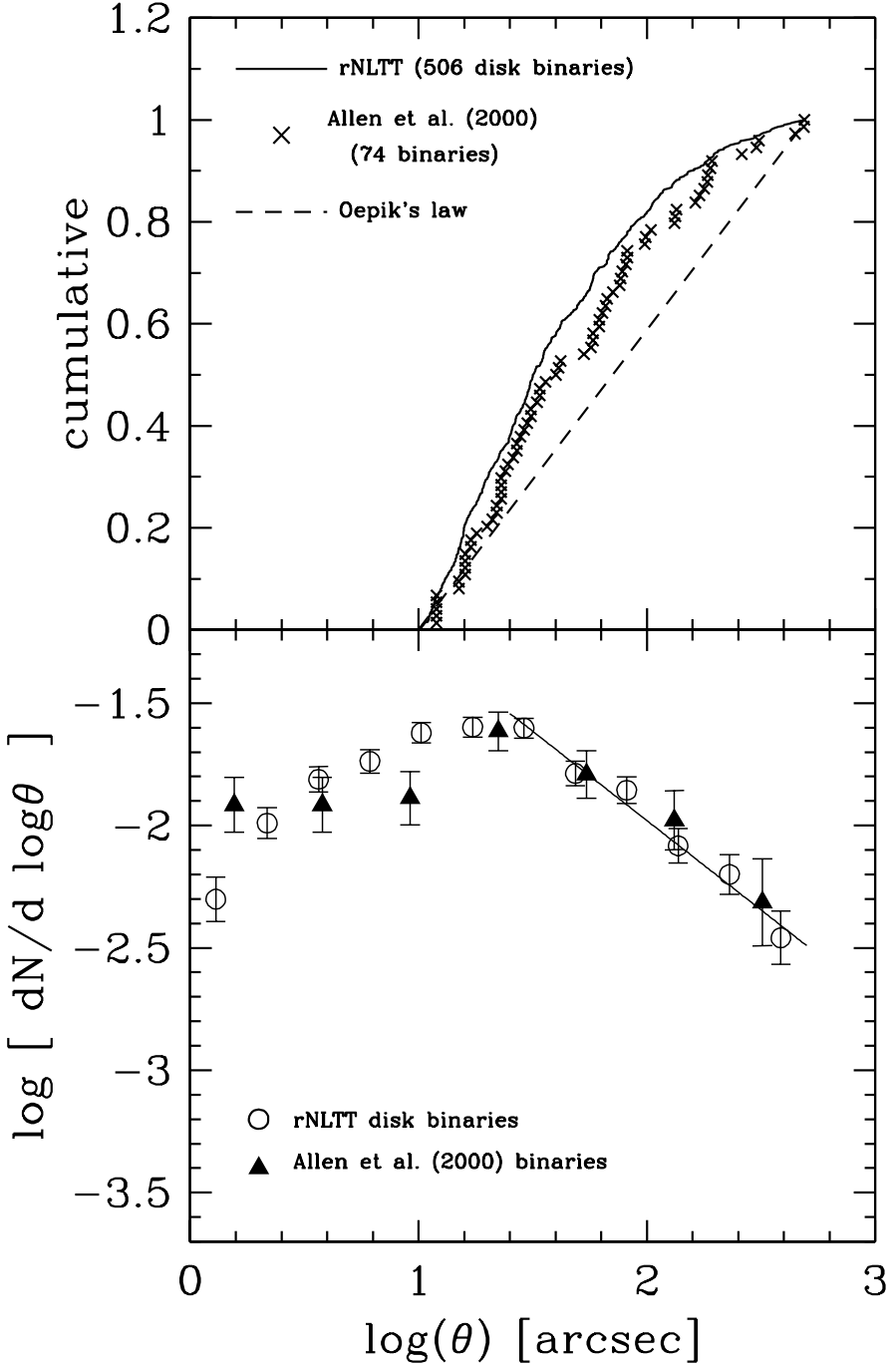


Fig. 15.— Distributions of angular separations for the Allen et al. (2000) sample of binaries in comparison with that of the disk binaries of the present work. The upper panel shows the respective cumulative distributions for all binaries wider than $10''$: both samples follow similar distributions, but very different than Oepik's law, which is represented as the dashed line. The lower panel shows the distributions of the complete samples in differential log-log form, where it can be seen that they match very well.